

AFIT/GAE/ENY/93D-3

**AD-A273 915**



**DTIC**  
ELECTE  
DEC 20 1993  
**S E D**

**EVALUATION OF A CONCENTRATION  
PROBE FOR APPLICATION IN A  
SUPERSONIC FLOW FIELD**

**THESIS**

**John S. Alsup, B.S.  
Captain, USAF  
AFIT/GAE/ENY/93D-3**

**93-30453**



Approved for public release; distribution unlimited

**93 12 15 07 9**

Disclaimer Statement

"The views expressed in the thesis are those of the author and do not reflect the official policy or position of the Department of Defense or the U.S. Government."

John Stevan Alsup

Accession For	
NTIS CRA&I	<input checked="checked" type="checkbox"/>
DTIC TAB	<input type="checkbox"/>
Unannounced	<input type="checkbox"/>
Justification .....	
By .....	
Distribution /	
Availability Codes	
Dist	Avail and/or Special
A-1	

DTIC QUALITY INSPECTED 1

AFIT/GAE/ENY/93D-3

EVALUATION OF A CONCENTRATION PROBE FOR APPLICATION  
IN A SUPERSONIC FLOW FIELD

THESIS

Presented to the Faculty of the Graduate School of  
Engineering of the Air Force Institute of Technology  
Air University

In Partial Fulfillment of the  
Requirements for the Degree of  
Master of Science in Aeronautical Engineering

John S. Alsup, B.S.  
Captain, USAF

December 1993

Approved for public release; distribution unlimited

## Acknowledgements

At this moment in time, as I reflect on the past and look to the future, I wish to pause and give thanks to all those people who have guided me along the way.

My deepest feelings of gratitude go to my Heavenly Father who gave me the strength and courage to press forward when nothing seemed to be going right.

Top of the list of people who I wish to thank is my thesis advisor, Dr. William Elrod. I'm grateful for his patience and guidance over unforeseen obstacles and his ability to use this thesis as a teaching tool. In Addition, I'd like to thank Dr. Paul King and Major Jerry Bowman for their expert advice and interest in my progress.

I send a multitude of thanks to the laboratory personnel, in particular, Mr. Andy Pitts, for his "can do" attitude. Whenever I needed assistance I could count on Andy to help in any possible way.

Finally, I give thanks to my wife, Heidi, and my children, Jeremy, Ryan, and Courtney, for their moral support and tolerance of both my physical and mental absence.

John Stevan Alsup

## Table of Contents

	Page
Acknowledgements . . . . .	ii
List of Figures . . . . .	v
List of Symbols . . . . .	vii
Abstract . . . . .	xi
I. Introduction . . . . .	1
1.1 Background . . . . .	1
1.2 Objectives and Scope . . . . .	3
II. Theory of Probe Operation . . . . .	4
III. Experimental Facility . . . . .	10
3.1 Concentration Probe System . . . . .	10
3.2 Mixture Supply System . . . . .	11
3.2.1 Constituent Metering Subsystem . . . . .	11
3.2.2 Mixing Chamber Subsystem . . . . .	13
3.3 Steady Flow Test System . . . . .	14
3.3.1 Stilling Chamber Subsystem . . . . .	15
3.3.2 Nozzle Subsystem . . . . .	16
3.3.3 Observation Chamber Subsystem . . . . .	17
3.4 Data Acquisition System . . . . .	17
3.5 Tank Discharge System . . . . .	18
IV. Experimental Procedures . . . . .	19
4.1 Preliminary Test Procedures . . . . .	19
4.1.1 Venturi Calibration . . . . .	19

	Page
4.1.2 Wire Sensor Thermal Resistance Coefficient . . . . .	20
4.1.3 Pretest Checklist . . .	20
4.2 Probe Temperature Response and Pressure Response Evaluation Procedures . . . . .	21
4.2.1 Pressure Response . . .	21
4.2.2 Temperature Response . .	21
4.3 Tank Discharge Calibration Procedures . . . . .	22
4.4 Steady Flow Calibration Procedures .	23
V. Results . . . . .	25
5.1 Probe Pressure and Temperature Response . . . . .	25
5.1.1 Probe Pressure . . . . .	25
5.1.2 Probe Temperature Response Results . . .	25
5.2 Tank Discharge Calibration Results .	32
5.3 Steady Flow Calibration Results . .	37
VI. Conclusions and Recommendations . . . . .	46
6.1 Conclusions . . . . .	46
6.2 Recommendations . . . . .	46
References . . . . .	48
Appendix A. Venturi Calibration . . . . .	49
Appendix B. Thermal Resistance Coefficient . . .	52
Vita . . . . .	53

## List of Figures

Figure	Page
1. Concentration Probe . . . . .	5
2. Mixture Supply System and Steady Flow Test System . . . . .	12
3. Mixing Chamber and Outlet End of Tube Core .	14
4. Stilling Chamber . . . . .	15
5. Supersonic Nozzle . . . . .	16
6. Tank Discharge System . . . . .	18
7. Chamber Pressure Response . . . . .	26
8. Chamber Temperature vs. Time . . . . .	26
9. Heat Directed on Side of Probe Cap, Shielded with Vacuum On . . . . .	28
10. Heat Directed on Side of Probe Cap, Shielded with Vacuum Off . . . . .	29
11. Heat Directed into Probe Chamber, No Shielding with Vacuum On . . . . .	30
12. Heat Directed into Probe Chamber, No Shielding with Vacuum Off . . . . .	30
13. Effect of Hot Wire Sensor on Chamber Temperature . . . . .	31
14. Tank Discharge Calibration Results Plotted using Equation 18 . . . . .	33
15. Pressure Effect, Tank Discharge Method . . .	35
16. Tank Discharge Calibration Results Plotted using Equation 19 . . . . .	36
17. Steady Flow Calibration Results ( $\epsilon = 1.131$ ) .	38
18. Steady Flow Calibration Results ( $\epsilon = 2.778$ ) .	38
19. Temperature vs. Helium Concentration ( $\epsilon = 1.131$ ) . . . . .	40

Figure	Page
20. Temperature vs. Helium Concentration ( $\epsilon = 2.778$ ) . . . . .	40
21. Comparison of Results of Tank Discharge Method and Steady Flow Method (Equation 18) .	41
22. Steady Flow Results ( $\epsilon = 1.131$ ), Plotted using Equation 19 . . . . .	43
23. Steady Flow Results ( $\epsilon = 2.778$ ), Plotted using Equation 19 . . . . .	43
24. Comparison of Tank Discharge Results and Steady Flow Results (Equation 19) . . . . .	45
25. Sensor Resistance vs. Temperature . . . . .	52



# List of Symbols

Symbol	Definition	Units
Roman Symbols		
A	calibration constant	ND
a	cross sectional area of the venturi throat	m <sup>2</sup>
A*	throat area of probe's sonic orifice	m <sup>2</sup>
A <sub>e</sub>	nozzle exit area	m <sup>2</sup>
A <sub>hw</sub>	probe chamber cross sectional area at location of hot wire sensor	m <sup>2</sup>
A <sub>ref</sub>	surface area of hot wire sensor	m <sup>2</sup>
A <sub>t</sub>	nozzle throat area	m <sup>2</sup>
B	calibration constant	ND
C	calibration constant	ND
C <sub>d</sub>	discharge coefficient (Eq. 20)	ND
C <sub>d vent</sub>	discharge coefficient of venturi (Eq. 29)	ND
C <sub>p</sub>	specific heat at constant pressure	ND
d	diameter of square-edged orifice or venturi throat	m
D	diameter upstream of flow measuring device	m
d <sub>w</sub>	diameter of hot wire sensor	m
E	calibration constant	ND
F	variable used to calculate discharge coefficient (Eq. 24)	ND
g <sub>c</sub>	proportionality constant	$\frac{\text{kg-m}}{\text{N-s}^2}$

Symbol	Definition	Units
$h$	heat transfer coefficient of hot wire sensor	$\frac{N}{s-m^2-K}$
$I$	current	amperes
$K$	flow coefficient (Eq. 21)	ND
$K_0$	limiting value of $K$ for values of $D$ and $\beta$ when $R_0 = 10^4 d/15$ (Eq. 23)	ND
$k_f$	thermal conductivity of fluid	$\frac{N}{s-m^2-K}$
$K_0$	limiting value of $K$ for values of $D$ and $\beta$ when $R_0$ becomes extremely large (Eq. 22)	ND
$M$	Mach number	ND
$\bar{m}$	molecular weight	$\frac{kg}{kmole}$
$\dot{m}$	mass flow rate of mixture	kg/s
$\dot{m}_{orifice}$	actual mass flow rate of air (Eq. 25)	kg/s
$\dot{m}_{thvent}$	theoretical mass flow rate of helium (Eq. 27)	kg/s
$Nu$	Nusselt number	ND
$P_0$	pressure of helium in discharge tank	$N/m^2$
$P_{mix}$	pressure of mixture in discharge tank	$N/m^2$
$P_0$	total pressure	$N/m^2$
$Pr$	Prandtl number	ND
$P_1$	pressure upstream of flow measuring device	$N/m^2$
$P_2$	pressure downstream of flow measuring device	$N/m^2$
$Q$	heat transfer rate	watts

Symbol	Definition	Units
$r$	ratio of pressures, $p_2/p_1$	ND
$R_b$	bridge circuit series resistance	ohms
$R_d$	Reynolds number at square-edged orifice	ND
$R_u$	universal gas constant of mixture	$\frac{N-m}{kg-^{\circ}K}$
$R_o$	sensor resistance at operating temperature	ohms
$Re$	Reynolds number of mixture	ND
$T$	static temperature	$^{\circ}C$
$T_f$	fluid temperature	$^{\circ}C$
$T_{so}$	temperature of helium in discharge tank	$^{\circ}C$
$T_m$	mean film temperature	$^{\circ}C$
$T_{mix}$	temperature of mixture in discharge tank	$^{\circ}C$
$T_o$	total temperature	$^{\circ}C$
$T_w$	hot wire operating temperature	$^{\circ}C$
$V$	velocity	m/s
$V_{br}$	bridge supply voltage	volts
$Y$	expansion factor (Eq. 28)	ND
$y$	calibration curve	ND
$Y_1$	net expansion factor (Eq. 26)	ND
$x$	species molar fractions	ND
$x_{so}$	molar fraction of helium	ND
$z$	$1 - p_2/p_1$	ND

Symbol	Definition	Units
Greek Symbols		
$\beta$	ratio of orifice plate diameter or venturi throat diameter to inlet diameter	ND
$\gamma$	ratio of specific heats	ND
$\gamma_m$	ratio of specific heats of mixture	ND
$\epsilon$	ratio of nozzle exit area to nozzle throat area	ND
$\mu$	dynamic viscosity of mixture	$\frac{\text{N-s}}{\text{m}^2}$
$\rho$	density of mixture	$\text{kg/m}^3$
$\rho_1$	density of fluid upstream of flow measuring device	$\text{kg/m}^3$
$\phi$	coefficient used to determine $k_r$ and $\mu$	ND

Abstract

Aspirating, concentration probes are used to measure binary gas concentrations in a supersonic flow. In the past, a tank discharge method has been used to calibrate concentration probes. An alternate calibration method has been developed and tested on a probe in a steady, subsonic/sonic flow. This study evaluated the calibration and performance of a concentration probe in a steady, supersonic flow over a range of mixture ratios of air and helium. The results of this study and a comparison of the two calibration methods are presented.

# EVALUATION OF A CONCENTRATION PROBE FOR APPLICATION IN A SUPERSONIC FLOW FIELD

## I. Introduction

Ramjet propulsion at hypersonic speed requires supersonic combustion for optimum performance. Supersonic combustion requires a high mixing rate of the fuel and air. In order to determine the mixing rate and degree of mixing, a probe may be inserted into the flowing binary fuel/air mixture. However, the probe requires calibration and its performance must be consistent.

### 1.1 Background

Early work using hot wire anemometer probes to measure binary gas concentrations was conducted by Adler (Adler, 1971:163). He observed that the heat loss from a hot wire sensor is a function of four properties: (1) velocity, (2) pressure, (3) temperature, and (4) composition. Moreover, he concluded that hot wire anemometers are useful as concentration sensitive instruments, having the following desirable characteristics: (i) quick response; (ii) continuous recording; (iii) point wise measurement in the field. These characteristics are important in the measurement of mixing rates in supersonic flow.

Many concentration probes have been designed and tested in the past. Blackshear and Fingerson designed a probe "to detect concentration fluctuations in a heated air jet mixing in air" (Blackshear and Fingerson, 1962:1709). Brown and Rebello employed a probe to determine the composition of a binary gas stream composed of two different gases (Brown and Rebello, 1972:649). In both cases, calibration curves were generated from data obtained using a tank discharge calibration method.

All the work up to this point was performed with subsonic flow fields. Ng was one of the first to use an aspirating, hot-film probe to determine the gas concentrations in supersonic flows (Ng and others, 1989:2,3). Likewise, he employed a tank discharge calibration method. His calibration method involved filling a tank to approximately 0.2 MPa then evacuating the tank's contents in incremental pressure steps. At each pressure step, a calibration point was derived. In the late 1980's, Tanis designed and built an aspirating hot wire probe for the study of supersonic turbulent shear layer mixing (Tanis, 1993). Tanis' probe is similar in design to Ng's probe with the exception that Tanis' probe contains a thermocouple and pressure port. Like those before him, Tanis generated calibration curves from data obtained using a tank discharge method.

In 1989, Stoller used Tanis' probe design to develop an alternate calibration technique in a steady, subsonic/sonic

flow field (Stoller, 1989). In this technique, unlike the tank discharge calibration method, the probe is calibrated in an environment in which it may actually be applied.

## 1.2 Objectives and Scope

This investigation evaluates the performance of Tanis' probe and examines the influence of flow properties on its calibration in a supersonic flow.

The goal of this work has been to:

1. Evaluate the aspirating concentration probe, designed by Tanis, for use in a supersonic binary flow field.
2. Calibrate the probe in a supersonic binary flow field using a steady flow calibration method.
3. Compare calibration results using the steady flow method to those obtained using a tank discharge method.

In this study, the probe was operated in a supersonic flow field where the ratio of nozzle exit area to throat area was 1.131 or 2.778. The concentration of the operating fluid ranged from 100 percent air to 100 percent helium. The Reynolds number in the probe chamber varied from 0.5 to 2.5, while the probe chamber pressure varied from 27.6 KPa to 41.4 KPa.



## II. Theory of Probe Operation

The heart of the probe is the hot wire sensor. The hot wire sensor is a strand of tungsten wire located in the probe sensor chamber and maintained at a constant temperature well above the fluid temperature. The heat transfer rate between the wire sensor and fluid is governed by the equation

$$Q = I^2 R_w = h A_{ref} (T_w - T_f) \quad (1)$$

where  $Q$  is the heat transfer rate,  $I$  is the current through the hot wire sensor,  $R_w$  is the operating resistance of the hot wire sensor,  $h$  is the heat transfer coefficient of the hot wire sensor,  $A_{ref}$  is the wire sensor surface area,  $T_w$  is the operating temperature of the hot wire sensor, and  $T_f$  is the fluid temperature. The heat transfer rate,  $Q$ , may be rewritten in the form

$$Q = \frac{V_{br}^2 R_w}{(R_w + R_b)^2} \quad (2)$$

where  $V_{br}$  is the bridge voltage and  $R_b$  is the bridge circuit series resistance. In this form, a knowledge of the heat transfer coefficient is not required to calculate the heat transfer rate.

As previously stated on page 1, the heat transfer of the sensor is a function of four properties:

(1) temperature, (2) pressure, (3) velocity, and (4) composition. The total temperature and total pressure are measured by a thermocouple and pressure port (connected to a pressure transducer), respectively located in the probe chamber, as shown in Figure 1. The third property, velocity, is derived from measured mass flow rate. This is accomplished by keeping the pressure behind the sonic orifice at approximately 3.5 KPa (vacuum level maintained by probe vacuum pump) to insure the orifice is choked. With total temperature and total pressure known, the mass flow rate through the choked orifice is calculated with the equation

$$\dot{m} = \frac{P_0 A^*}{\sqrt{T_0}} \sqrt{\frac{\gamma_B}{R_B} \left( \frac{2}{\gamma_B + 1} \right)^{\frac{\gamma_B + 1}{\gamma_B - 1}}} \quad (3)$$

where  $P_0$  is the total pressure in the probe chamber,  $T_0$  is

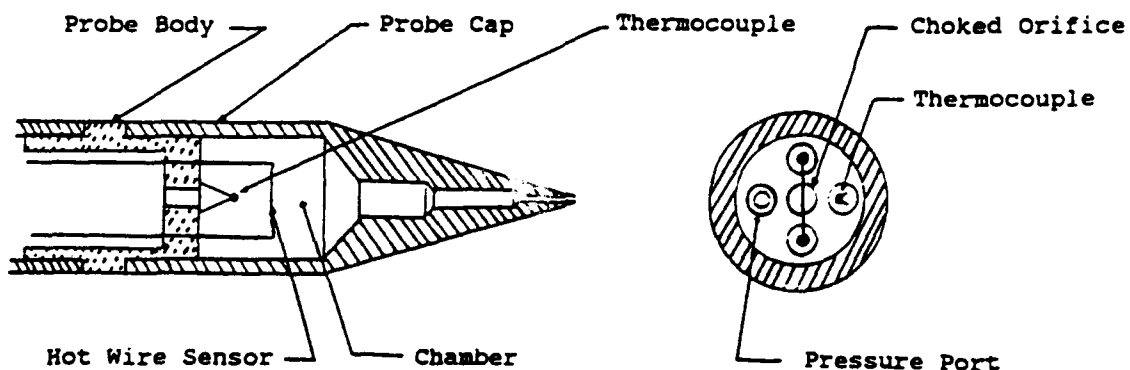


Figure 1. Concentration Probe

the total temperature in the probe chamber, and  $A^*$  is the throat area of the sonic orifice (Shapiro, 1953:85).

Equation 3 assumes the discharge coefficient of the sonic orifice is one. The velocity is derived from the mass flow rate (assuming uniform flow) by the expression

$$V = \frac{\dot{m}}{\rho A_{hw}} \quad (4)$$

where  $\rho$  is the density of the gas in the probe chamber and  $A_{hw}$  is the cross sectional area of the probe chamber at the hot wire sensor location. With three of the four properties known, the fourth property, the molar concentration (composition) can be isolated and determined.

Referring to Equation 1, the heat transfer coefficient,  $h$ , can be derived from the non-dimensional Nusselt number in the form

$$Nu = \frac{h d_w}{k_f} \quad (5)$$

where  $d_w$  is the sensor wire diameter and  $k_f$  is the thermal conductivity of the fluid evaluated at the mean film temperature,  $T_m$ . The mean film temperature is expressed by

$$T_m = \frac{T_w + T_f}{2} \quad (6)$$

The determination of fluid properties at the film temperature does not eliminate the temperature loading,  $T_w/T_f$  (i.e., A low temperature loading avoids complications due to temperature dependence of the fluid properties). However, the residual effect of temperature loading is assumed negligible and essentially independent of Reynolds number (Collis and Williams, 1959:365,366).

By combining Equations 1 and 5, the Nusselt number takes on the form

$$Nu = \frac{Qd_w}{k_f A_{ref} (T_w - T_f)} \quad (7)$$

If Equations 2 and 7 are combined the result is

$$Nu = \frac{V_{br}^2 R_w d_w}{k_f A_{ref} (T_w - T_f) (R_w + R_b)^2} \quad (8)$$

Equation 8 is useful since all the required parameters, except  $k_f$ , are known or measurable. For a binary gas mixture, the thermal conductivity,  $k_f$ , is determined by a modified version of Wilke's semiempirical equation

$$k_f = \sum_{i=1}^n \frac{x_i k_i}{\sum_{j=1}^n x_j \phi_{ij}} \quad (9)$$

where

$$\phi_{ij} = \frac{1}{\sqrt{8}} \left(1 + \frac{\bar{m}_i}{\bar{m}_j}\right)^{-1/2} \left[1 + \left(\frac{\mu_i}{\mu_j}\right)^{1/2} \left(\frac{\bar{m}_j}{\bar{m}_i}\right)^{1/4}\right]^2 \quad (10)$$

Likewise, the binary gas viscosity is given by

$$\mu = \frac{\sum_{i=1}^n \frac{x_i \mu_i}{\sum_{j=1}^n x_j \phi_{ij}}} \quad (11)$$

In Equations 9, 10, and 11, the variables  $x_i$  and  $x_j$  are species molar fractions,  $k_i$  is the thermal conductivity of an individual gas,  $\mu_i$  and  $\mu_j$  are the viscosities for the individual gases, and  $\bar{m}_i$  and  $\bar{m}_j$  are the species individual molecular weights. These equations are applicable to low-density gases (Bird, 1960:24,258).

In the past, the Nusselt number has been related to King's law. One form of King's law given by Collis and Williams for the average heat transfer rate from an infinite cylinder is presented as

$$Nu = \frac{1}{\pi} + \sqrt{\frac{2RePr}{\pi}} \quad (12)$$

where  $Re$  is the Reynolds number and  $Pr$  is the Prandtl number (Collis and Williams, 1959:361). The Reynolds number is defined by

$$Re = \frac{\rho d_v}{A_{He} \mu} \quad (13)$$

and the Prandtl number by

$$Pr = \frac{C_p \mu}{k} \quad (14)$$

where  $C_p$  is the specific heat, and  $\mu$  is the fluid viscosity evaluated at the film temperature.

In his work, Tanis developed Equation 15 which relates mole fraction of helium to Reynolds number.

$$Nu \left(1 + \frac{T_g}{T_f}\right)^{0.17} Pr^{-0.3} (1 + X_{He})^{(0.55 - 0.13 Re)} = A + B Re^{0.45} \quad (15)$$

$X_{He}$  is the helium molar concentration and the variables A and B are calibration constants (Tanis, 1993:59). This equation is similar to previously proposed equations with the exception that Tanis' equation accounts for variations in concentration.

### III. Experimental Facility

For this study, a test facility was established to create a steady, supersonic flow field with mixture ratios of helium and air variable from 100 percent air to 100 percent helium. The test facility is capable of varying the mass flow rates of both the air and helium sources, mixing the two gases together, then expelling the mixed gases through a convergent - divergent nozzle. In addition, provisions were made to regulate the pressure aft of the convergent - divergent nozzle, thus, controlling the expansion of the jet exiting the divergent section of the nozzle.

The test facility consists of five systems: (1) concentration probe system, (2) mixture supply system, (3) steady flow test system, (4) data acquisition system, and (5) tank discharge system.

#### 3.1 Concentration Probe System

The concentration probe, shown in Figure 1 on page 5, was designed by Tanis. The probe's removable, brass, cone shaped cap has a 0.343 mm diameter opening at the forward end. The opening expands in steps to a chamber 2.56 mm in diameter. Contained within this chamber are a 0.0127 mm (0.0005 in) diameter tungsten hot wire sensor, a K type (Chromel - Alumel) thermocouple wired to an electronic ice point, a 0.508 mm diameter pressure port, and a 0.508 mm

diameter sonic orifice. The tungsten wire is bridged between two #16 sewing needles (maximum needle diameter is 0.409 mm) which are epoxied into the probe's brass body. Wires soldered to the aft end of the sewing needles are connected via cabling to a TSI intelligent flow analyzer (IFA-100). The pressure port has a 0.508 mm (OD), outside diameter, hypodermic tube pressed into it. The hypodermic tube extends back approximately 10 cm at which point it is inserted into and soldered to a 0.914 mm (OD) tubing. This tubing extends back approximately 33 cm where it terminates at a pressure transducer. Behind the sonic orifice, the pressure is maintained below 3.5 KPa (pressure is absolute unless otherwise indicated), by a vacuum pump. The aft end of the probe body is glued to a stainless steel tube 3.175 mm (OD) and 35.7 cm in length, through which the probe wiring, tubing and vacuum suction is drawn.

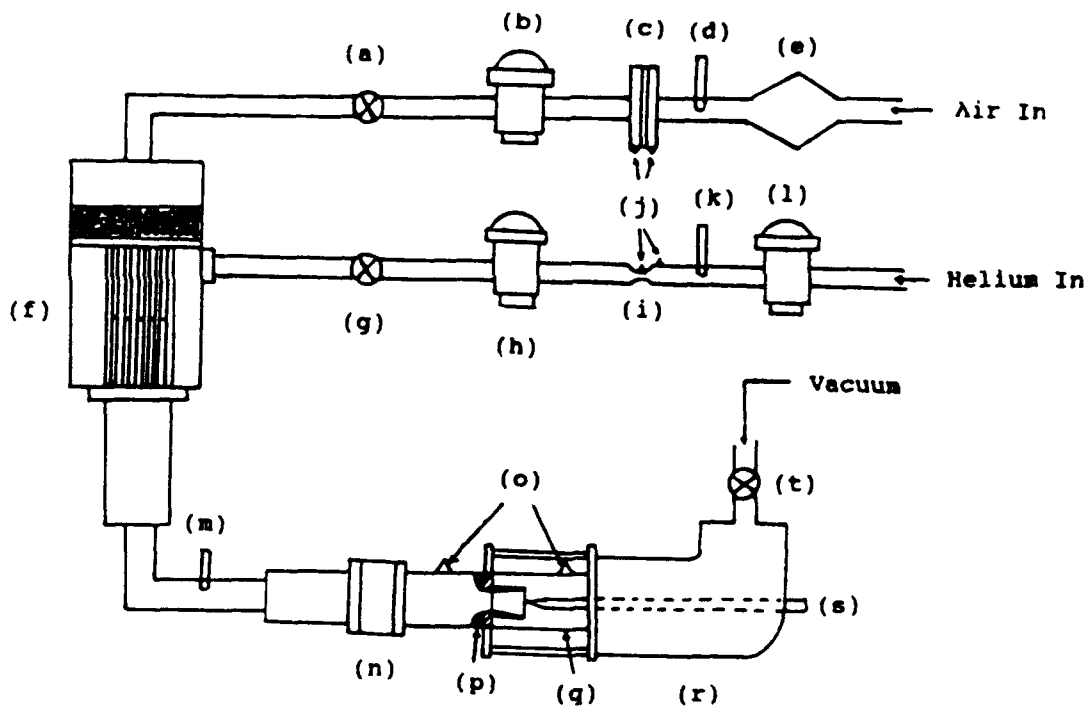
### 3.2 Mixture Supply System

Both the mixture supply system and the steady flow test system are shown in Figure 2. The mixture supply system is further broken down into the constituent metering subsystem and the mixing chamber subsystem.

3.2.1 Constituent Metering Subsystem. Air is supplied to the test facility by means of an air compressor maintained at a pressure of approximately 0.7 MPa. The compressed air is filtered through paper coffee filters and a cyclone separator, (e), prior to passing through a square-



edged orifice, (c). The square-edged orifice flow measuring system is equipped with two pressure transducers, (j), and a thermocouple, (d), to obtain the data required to calculate the mass flow rate of air entering the mixing chamber. The square-edged orifice location (and venturi location in the helium line) meets ASME recommended minimum lengths of pipe between the orifice (or venturi tube) and control valves (ASME, 1971:180).



(a)&(g) solenoid valves; (b),(h)&(l) dome valves;  
(c) square-edged orifice; (d),(k)&(m) thermocouples;  
(e) paper filters and cyclone separator; (f) mixing chamber;  
(i) venturi; (j)&(o) pressure transducers; (n) stilling  
chamber; (p) supersonic nozzle; (q) observation chamber;  
(r) probe holder; (s) probe; (t) globe valve

Figure 2. Mixture Supply System and Steady Flow Test System

Before enter the mixing chamber, the air pressure is regulated by a dome valve, (b), to control the mass flow rate of air.

Helium is supplied to the test facility by bottles of compressed helium. The helium pressure to the test facility is regulated by two dome valves, (h & l). The dome valves step the helium tank pressure from a maximum pressure of 15 MPa at the helium tanks to a maximum pressure of 0.5 MPa entering the mixing chamber. Between the two dome valves, a venturi tube, (i); two pressure transducers, (j); and a thermocouple, (k); are employed in obtaining data to determine the mass flow rate of helium entering the mixing chamber.

3.2.2 Mixing Chamber Subsystem. The mixing chamber, (f), was originally built by Zakanycz for use in studying the turbulent mixing of binary gases (Zakanycz, 1971). Figure 3 is Zakanycz's drawing of the chamber. The air enters the chamber at the forward end where it first impinges on a baffle. The air is then dispersed by a screen and glass beads. At the same time, helium enters the mixing chamber through a side boss where it is directed on a baffle which disperses the flow. The air and helium then enter interspersed parallel tubes (45 tubes for air, 52 tubes for helium). Streams of helium and air exit the tubes where they mix in tubing connecting the mixing chamber to the stilling chamber.

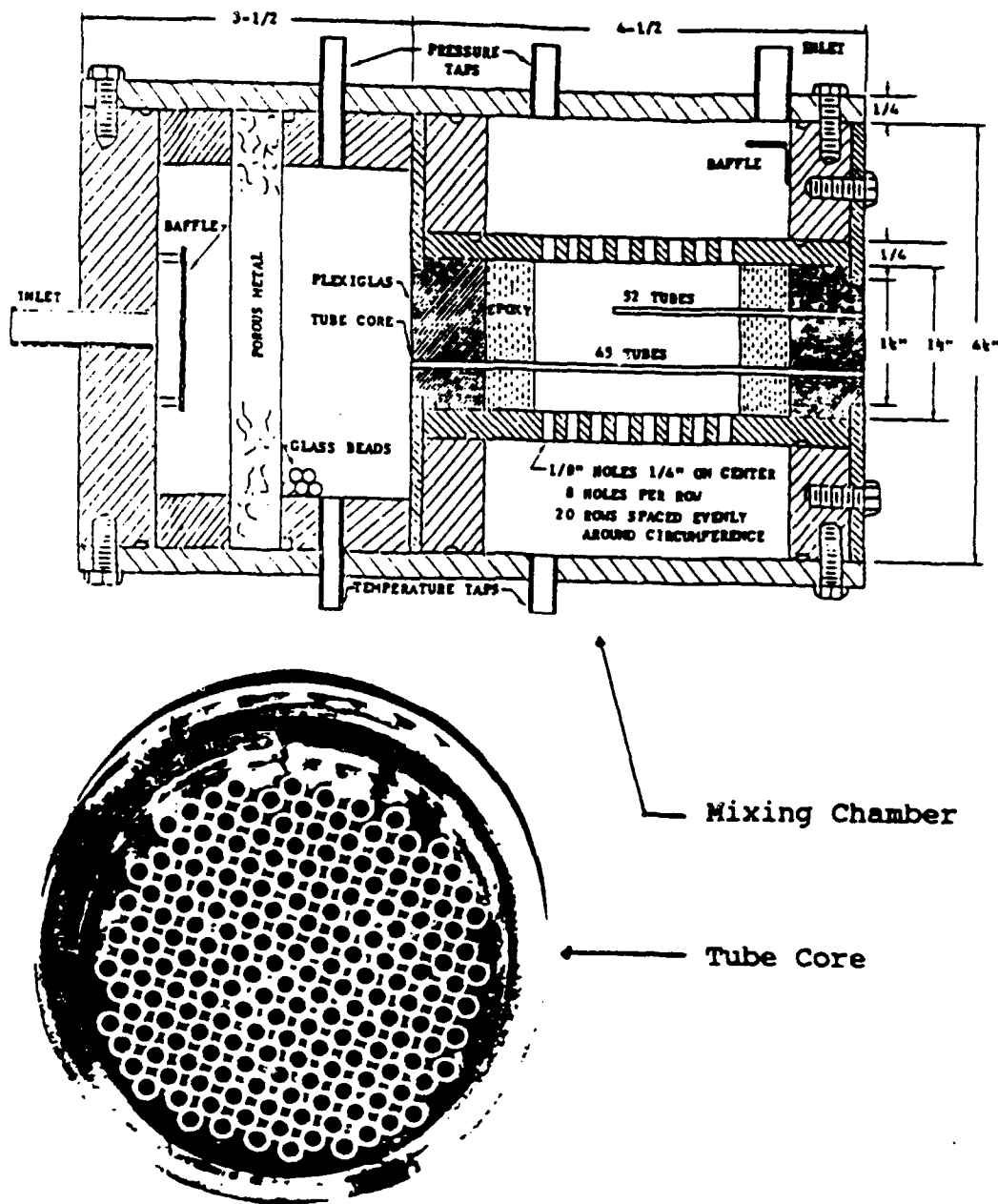


Figure 3. Mixing Chamber and Outlet End of Tube Core

### 3.3 Steady Flow Test System

The steady flow test system is further divided into the stilling chamber subsystem, the nozzle subsystem, and the observation chamber subsystem.

3.3.1 Stilling Chamber Subsystem. The stilling chamber, Figure 4 and (n) in Figure 2 page 12, serves the purpose of creating a uniform flow prior to the flow entering the nozzle. Moreover, the stilling chamber is equipped with a pressure transducer for determining the total pressure of the binary gas. Just upstream of the stilling chamber, a thermocouple measures the total temperature of the flow.

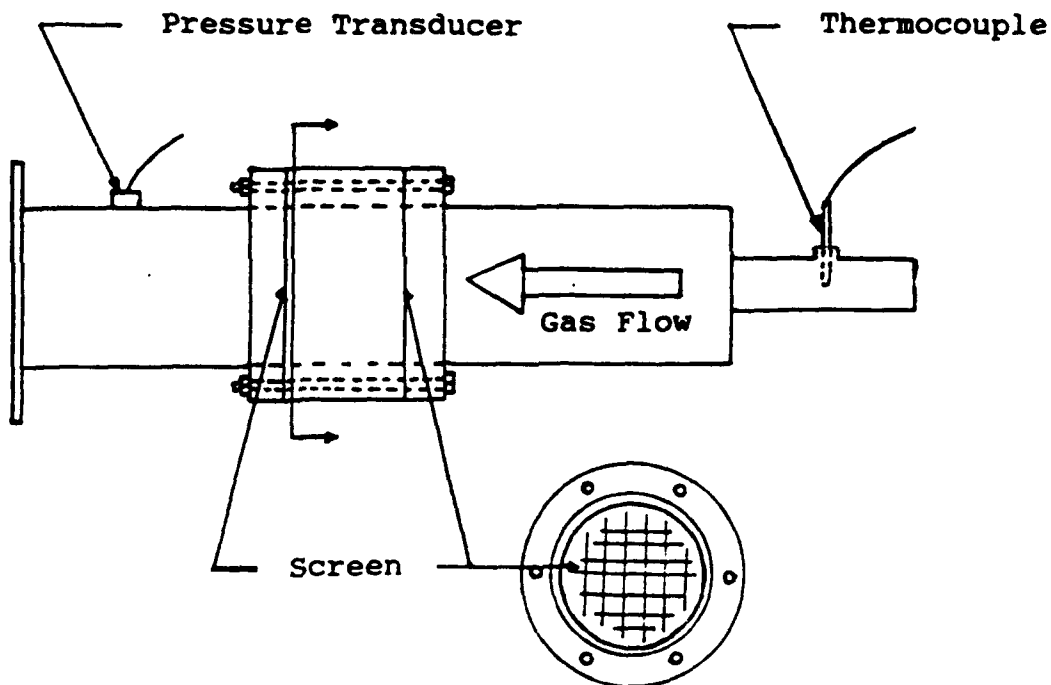


Figure 4. Stilling Chamber

3.3.2 Nozzle Subsystem. The nozzle, Figure 5 and (p) in Figure 2 page 12, is an axisymmetric convergent - divergent nozzle with a permanent convergent section and a removable divergent section. The convergent section of the nozzle has a smooth, convex shape (with a ratio of inlet area to throat area of approximately 7.87) while the divergent section's interior surface has a conical shape. The divergent section of the nozzle can be removed and replaced with another divergent section to vary the ratio of exit area to throat area,  $\epsilon$ , from 1 to 2.778.

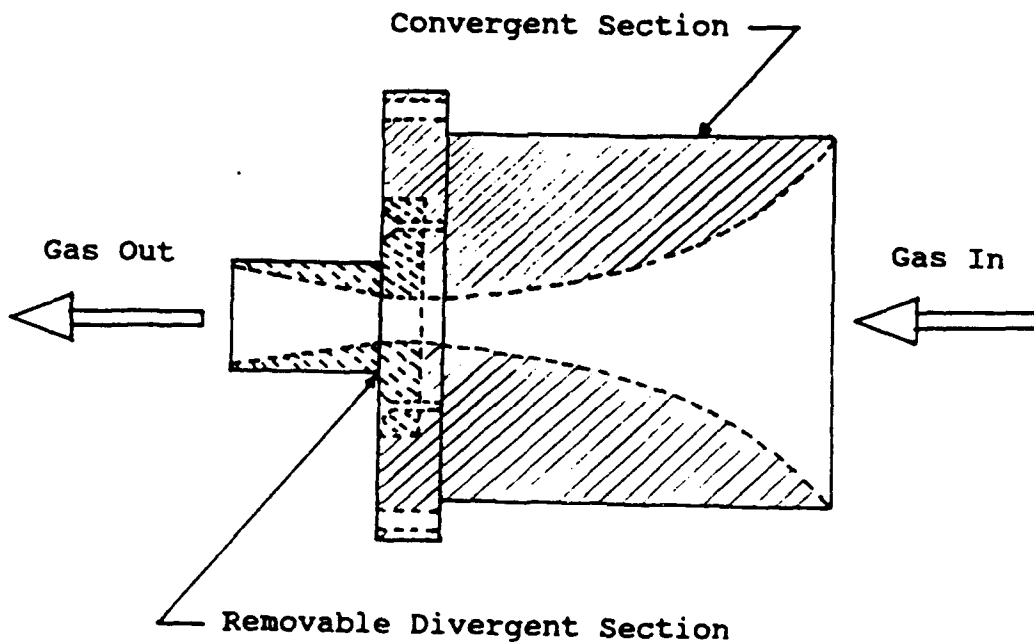


Figure 5. Supersonic Nozzle

3.3.3 Observation Chamber Subsystem. The observation subsystem consists of a plexiglass observation chamber, (q) in Figure 2, probe holding structure, (r) in Figure 2, and vacuum source. The observation chamber is plexiglass to allow visual positioning of the probe in the exit plane of the nozzle. In addition, the observation chamber is equipped with a pressure transducer to measure the back pressure. The probe holding structure keeps the probe fixed in the center of the exit plane of the nozzle. Moreover, it allows for back and forth adjustment parallel to the nozzle axis. The vacuum source consists of three vacuum pumps and sixteen aircraft fuel tanks which serve as a vacuum reservoir. The vacuum pressure in the observation chamber is controlled by a valve, (t) in Figure 2, just downstream of the probe holder.

#### 3.4 Data Acquisition System

The data acquisition system is a Nicolet 500 data acquisition system which interfaces with a 386 personal computer. The Nicolet 500 is capable of receiving and processing 20 signals. The test facility uses 10 of the signal channels. Four signals come from the four pressure transducers at the orifice plate and venturi tube. One channel receives data from the stilling chamber pressure transducer and another channel receives data from the thermocouple just upstream of the stilling chamber. One line is connected to the observation chamber pressure

transducer, while the last three signals originate from the probe hot wire sensor, probe thermocouple, and probe pressure transducer.

### 3.5 Tank Discharge System

The tank discharge apparatus used for the tank discharge calibration method is shown in Figure 6. The tank discharge apparatus consists of a cylindrical tank (16.5 cm in diameter and 19 cm in length) fitted with a K type thermocouple and a pressure transducer. Air and helium are introduced into the tank via needle valves and expelled from the tank via a ball valve. A plastic tube attached to the end of the ball valve and fitted over the probe cap allows the passage of the gas from the tank to the probe. The gas flows through the probe in the calibration process.

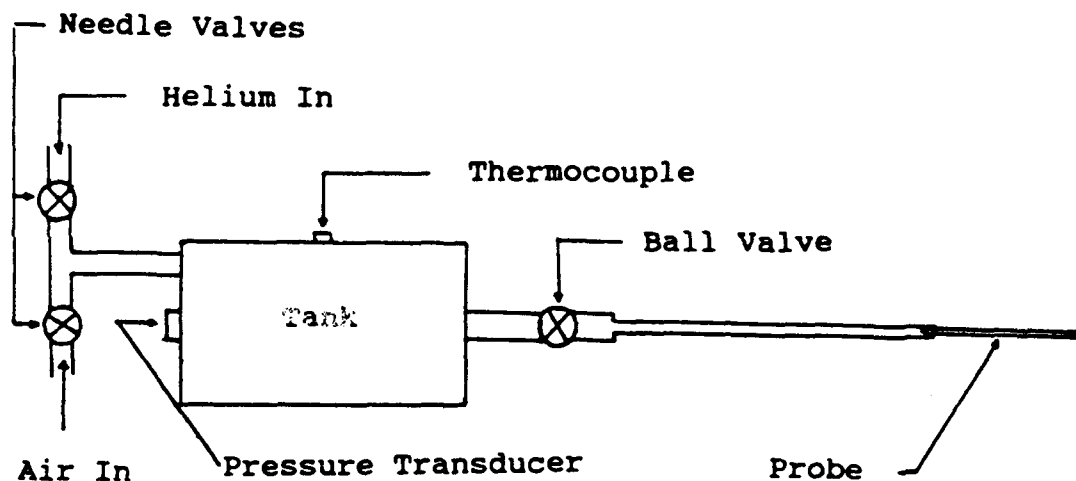


Figure 6. Tank Discharge System

#### IV. Experimental Procedures

Prior to testing and calibrating the probe, the venturi tube and pressure transducers had to be calibrated, and the sensor wire thermal resistance coefficient determined. The next section describes these preliminary test procedures while the following sections describe the probe response tests and calibration procedures. It has been determined from experience that each hot wire sensor has its own "personality"; therefore, the same hot wire sensor was used during all calibration procedures.

##### 4.1 Preliminary Test Procedures

4.1.1 Venturi Calibration. Before using a venturi to measure true mass flow rate, its discharge coefficient had to be determined. To do this, the venturi was placed in the air supply line approximately two meters downstream of the orifice plate, (c) in Figure 2. Since published literature contains significant discharge coefficient data on square-edged orifices based on Reynolds number, the orifice served as a reference in calibrating the venturi. The calibration procedure started by initiating a low mass flow rate of air flow through the system and recording pressure and temperature data from both the orifice and venturi. The mass flow rate of air was incrementally increased to give a range of Reynolds numbers. Calculated discharge coefficients greater than one were discarded and other



erroneous discharge coefficients were eliminated using Chauvenet's rejection criteria as discussed by Taylor (Taylor, 1982:142-4). Finally, the remaining discharge coefficients were averaged to determine the discharge coefficient. Appendix A contains the equations that were necessary to calculate the venturi discharge coefficient.

4.1.2 Wire Sensor Thermal Resistance Coefficient. The hot wire sensor is designed to function at a constant temperature. In order to determine the sensor operating temperature, the linear relationship between the sensor resistance and sensor temperature had to be investigated. This was accomplished by inserting the probe into a rubber stopper which was placed over the top of an insulated flask. The flask was then placed on a hot plate. The Nicolet 500 read and displayed the temperature in the probe by means of the probe thermocouple. At the same time, the IFA-100 displayed the sensor resistance. Temperature and resistance readings were taken approximately every 10°C over a range from 30°C to 80°C. Appendix B contains the plot of sensor temperature versus sensor resistance and the correlation factor of the data. The thermal resistance coefficient and overheat ratio were determined using procedures prescribed in the IFA-100 manual (IFA-100 Users Manual). An overheat ratio of 1.5 was chosen after personal conversation with Tanis.

4.1.3. Pretest Checklist. Prior to testing, a checklist was utilized to avoid mistakes in taking data.

The checklist included adjusting the pressure transducer signal conditioners to compensate for drift, turning on the thermocouple ice points, checking for leaks, and setting the overheat ratio.

#### 4.2 Probe Temperature Response and Pressure Response Evaluation Procedures

The probe chamber temperature and pressure response characteristics needed to be evaluated and understood before the probe was calibrated. The next two sub-subsections present ways in which the probe pressure response and temperature response were evaluated.

4.2.1 Pressure Response. The response of the probe to a step change in pressure was evaluated by turning on the probe vacuum system while sealing off the front entrance of the probe cap. After the probe chamber pressure stabilized, the cap entrance was abruptly opened. Simultaneously, the Nicolet 500 data acquisition system recorded the change in pressure with time.

4.2.2 Temperature Response. In the past, the probe was calibrated in subsonic/sonic flow where the static temperature was relatively constant. In a supersonic flow field, the static temperature decreases substantially with an increase in Mach number, as can be seen by Equation (16).

$$T = T_o (1 + \frac{\gamma - 1}{2} M^2)^{-1} \quad (16)$$

The temperature response was determined by introducing the probe to a Mach 2.56 ( $\gamma = 1.4$ ) flow field. The Nicolet 500 data acquisition system was actuated with no flow past the probe. A gas flow was then initiated by means of a solenoid valve. The data was recorded at 20 Hz for approximately 90 seconds. The procedure was repeated twice: once with a mixture of air and helium and then with pure helium. Further tests involved blowing hot air on the probe cap with the entrance of the cap shielded. Hot air was blown into the probe chamber (no shielding) to examine the influence of heat transfer on the data acquired with the probe. With both the probe vacuum and hot wire sensor on, a final test exposed the probe to the atmosphere to evaluate the effect of the hot wire sensor heat output on the chamber temperature versus time.

#### 4.3 Tank Discharge Calibration Procedures

The tank discharge method has been the calibration method of choice in the past. To begin the calibration procedure, the Nicolet 500 data acquisition was set up to record sensor bridge voltage, probe chamber pressure, and temperature. The operating resistance of the probe hot wire sensor was set for an overheat ratio of 1.5 ( $T_o = 152^\circ\text{C}$ ) and the probe vacuum was turned on. The tank was evacuated and then filled with air to approximately 140 KPa and connected to the probe via a short plastic tube. As the tank discharged, the Nicolet 500 data acquisition system recorded

4800 data points over a two minute period. The tank was prepared for another test by evacuating the tank and filling it with air to just below atmospheric pressure. After recording tank pressure and temperature, helium was added until the tank pressure reached a value corresponding to the desired mixture pressure, at which time the mixture pressure and temperature were recorded. The mole fraction of helium in the tank was calculated using the relationship:

$$X_{He} = \frac{P_{He} T_{mix}}{P_{mix} T_{He}} \quad (17)$$

For succeeding tests, the tank was evacuated to approximately 3.5 KPa (lowest consistent vacuum pressure obtained by vacuum pump) and then purged with air to remove any residual helium. The mixture pressure ratio was varied by reducing the air pressure, while the mixture pressure remained relatively constant. To obtain data with 100 percent helium, the tank was evacuated to approximately 3.5 KPa and purged with a stream of helium to remove as much residual air as possible.

#### 4.4 Steady Flow Calibration Procedures

The probe was calibrated using two supersonic nozzles. The Mach numbers established using the two nozzles ( $\gamma = 1.4$ ) were 1.43 ( $\epsilon = 1.131$ ) and 2.56 ( $\epsilon = 2.778$ ). The probe was inserted into the probe holding structure and positioned so that the extreme tip of the probe cap lay in the center of

the exit plane of the divergent nozzle. The Nicolet 500 was configured to a 50 Hz sampling rate over a four second sampling time and the IFA-100 was set for a overheat ratio of 1.5 ( $T_w = 152^{\circ}\text{C}$ ). Air flow was initiated and metered to obtain a predetermined probe chamber pressure.

Simultaneously, the back pressure in the observation chamber was adjusted via the vacuum control valve. Adjustment of the back pressure was necessary to obtain quasi-optimum expansion of the exiting gas jet. Once the desired probe chamber pressure and nozzle back pressure were established and the flow stabilized, the data acquisition system was initiated. After the data run was completed, the data was downloaded to files stored in the 386 personal computer.

The procedure was repeated three additional times for pure air, each time increasing the probe chamber pressure. The chamber pressure in the probe varied from 29 KPa to 40 KPa. This range was chosen to allow comparison between Stoller's subsonic/sonic results and the supersonic results of this study (Stoller, 1989). Next, helium was introduced to the system. The previous steps were followed for a range of air and helium concentrations. Prior to recording data for the tests with pure helium, the system was operated for a few seconds with pure helium to expel any residual air.

## V. Results

In this section, pressure and temperature response test results are presented and examined. After evaluation of the probe response test results, the results of the tank discharge calibration method and steady flow calibration method are examined and compared.

### 5.1 Probe Pressure and Temperature Response

The pressure and temperature response of the probe were investigated to determine the probe's performance in a dynamic situation (e.g., The probe is traversed in gases containing temperature and density gradients). The results of the pressure response test are presented first, followed by the temperature response test results. Pressure is absolute pressure unless otherwise indicated.

5.1.1 Probe Pressure Response Results. Figure 7 illustrates the probe response to a step change in pressure at its inlet from approximately 1.4 KPa to an atmospheric pressure of 97.9 KPa. The chamber pressure reaches 99 percent of its steady state value in 0.62 seconds after opening the chamber to atmospheric pressure. An additional test was conducted to determine the repeatability of the probe pressure response. The results of the second test were a duplicate of the first test.

5.1.2 Probe Temperature Response Results. Figure 8 shows the temperature response characteristics of the probe

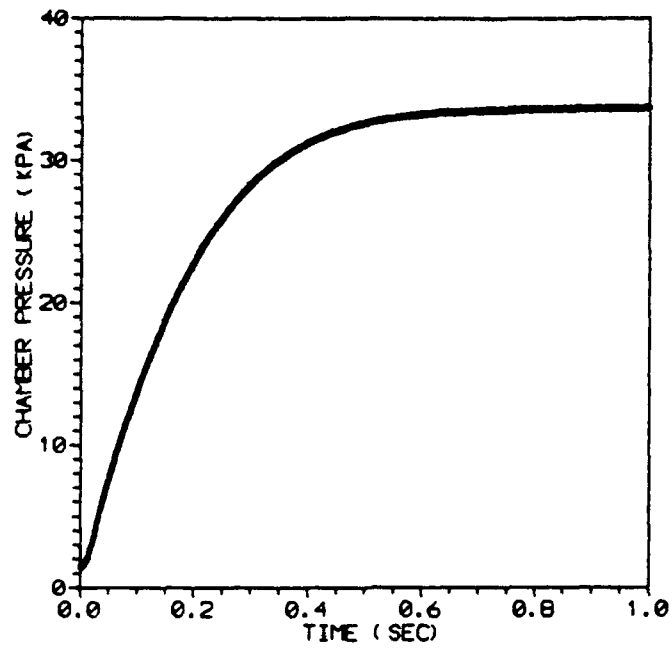


Figure 7. Chamber Pressure Response

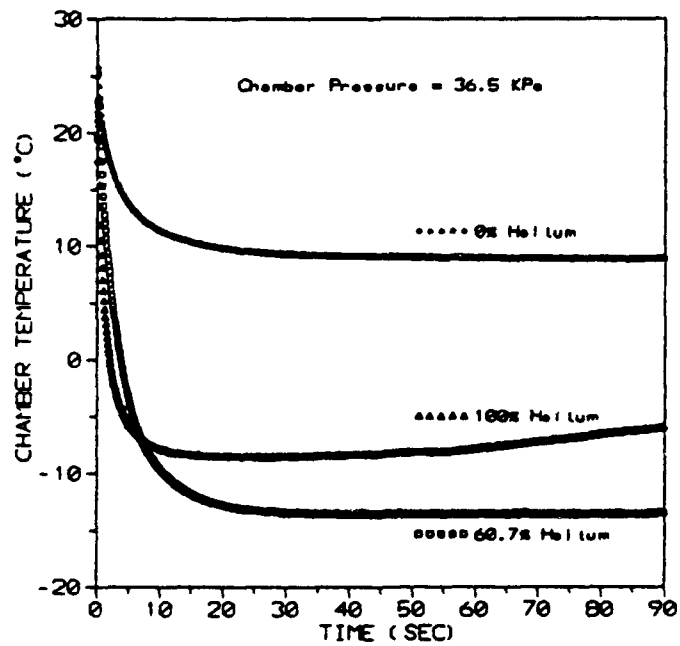


Figure 8. Chamber Temperature vs. Time

in a supersonic flow (nozzle  $\epsilon = 2.778$ ) with the probe vacuum on and the hot wire sensor off. A quick and stable temperature is critical for a concentration probe. The test results indicate that the chamber temperature reaches steady state within 25 seconds and remains stable. The temperature of the air/helium mixture (60.7 percent helium) increases after 55 seconds due to an increase in back pressure in the observation chamber. The back pressure increases from about 6.9 KPa at 55 seconds to 10.5 KPa at 90 seconds.

The test results also demonstrate the strong influence of the static temperature of the external flow field on the probe chamber temperature. The brass cap's high thermal conductivity and proximity to the chamber thermocouple all account for the strong influence of the cap temperature on the measured chamber temperature.

A test was conducted where the brass probe cap was heated with a hot air gun directed to the side of the probe cap and with the room air drawn into the probe (shielded from the hot air of the hot air gun). The test results are shown in Figure 9. The brass heats up quickly, radiating and convecting heat to the probe thermocouple. Prior to the addition of heat, the probe chamber temperature is lower than the atmospheric temperature. The lower temperature is attributed to air expanding from room ambient pressure to a lower pressure in the probe chamber. The expanded air cools the probe cap which in turn cools the chamber thermocouple. From the results of this test and



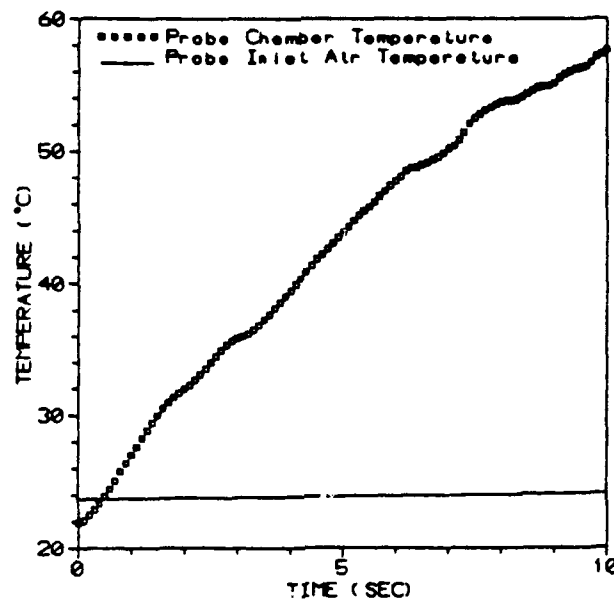


Figure 9. Heat Directed on Side of Probe Cap, Shielded with Vacuum On

following tests, the probe thermocouple is assumed to be sensing local total temperature or fluid temperature and not the total temperature of the flow prior to entering the probe. The difference in the total temperatures is due to heat transfer within the probe chamber.

Figure 10 shows the results when the previous test was repeated with the probe vacuum turned off. The results indicate that radiation heat transfer and convection heat transfer are significant between the probe cap and thermocouple.

Figures 11 and 12 were obtained by removing the shielding and directing a jet of hot air into the probe chamber. Test results shown in Figure 11 were with the

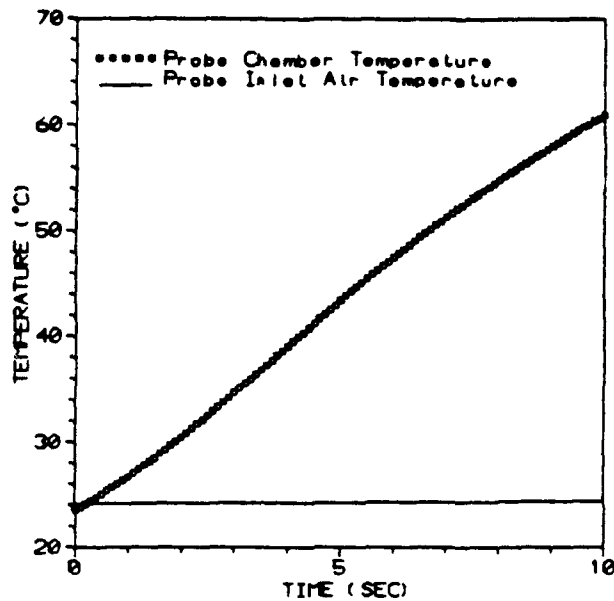


Figure 10. Heat Directed on Side of Probe Cap,  
Shielded with Vacuum Off

probe vacuum on, while the test results given in Figure 12 were with the probe vacuum off. With air being drawn into the probe (Figure 11), its chamber temperature is unstable due to turbulence in the chamber or to a non-uniform temperature air stream from the hot air gun at the probe entrance. However, in Figure 12 the chamber temperature is steadily increasing at a rate slower than the external hot air temperature. Results shown in Figure 11 are somewhat inconclusive due to the data scatter, but results shown in Figures 11 and 12 are consistent with the finding that the chamber thermocouple is sensitive to the temperature of the brass cap.

The previous tests presented in Figures 8 - 12 were conducted with the hot wire sensor inoperative. Figure 13

dem  
had  
exp  
tur  
sta  
sta  
and  
in  
the  
tem

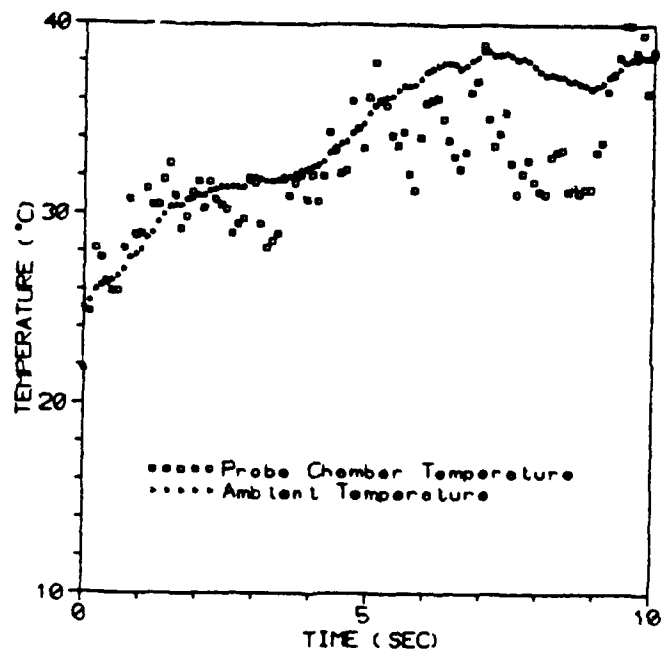


Figure 11. Heat Directed into Probe Chamber,  
No Shielding with Vacuum On

but  
mat  
the  
cou

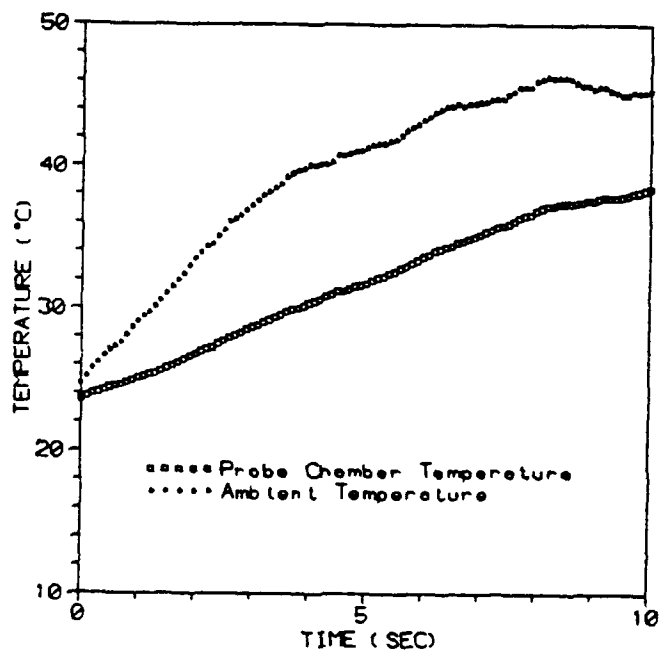


Figure 12. Heat Directed into Probe Chamber,  
No Shielding with Vacuum Off

F:

THIS  
PAGE  
IS  
MISSING  
IN  
ORIGINAL  
DOCUMENT

*Fig 13.*

## 5.2 Tank Discharge Calibration Results

The tank discharge calibration method was performed for comparison to the steady flow calibration method. During the calibration procedure, the probe temperature remained constant at 25°C (+2.5°C, -5°C).

Calibration curves were plotted using Equation 18 which is a modified version of Equation 15.

$$\underbrace{Nu(1+\frac{T_v}{T_f})^{0.17}}_{T1} \underbrace{Pr^{-0.3}(1+X_{No})^{(0.13Re-0.55)}}_{T2} = \underbrace{A+BRe^{0.65}+CRe^{0.9}+ERE^{1.35}}_{T3} \quad (18)$$

The difference is in the sign of the exponent of term T2 and the expansion of term T3. The exponents in Equation 15 are ones that occurred most often for Tanis during the calibration of his probe (Tanis, 1993:61). The tank discharge calibration results of this investigation, shown in Figure 14, are plotted with  $Re^{0.45}$  vs. the left side of Equation 18. The values in Figure 14 were obtained by taking 4800 points, then averaging every sequential group of 10 points. From these 480 average values, a data point was chosen at a chamber pressure of 41.4 KPa and at every 0.69 KPa chamber pressure step down to 27.6 KPa. The upper right points in each concentration grouping correspond to the higher chamber pressures while the lower left values correspond to the lower chamber pressures. The slopes for each group of concentrations are similar indicating the

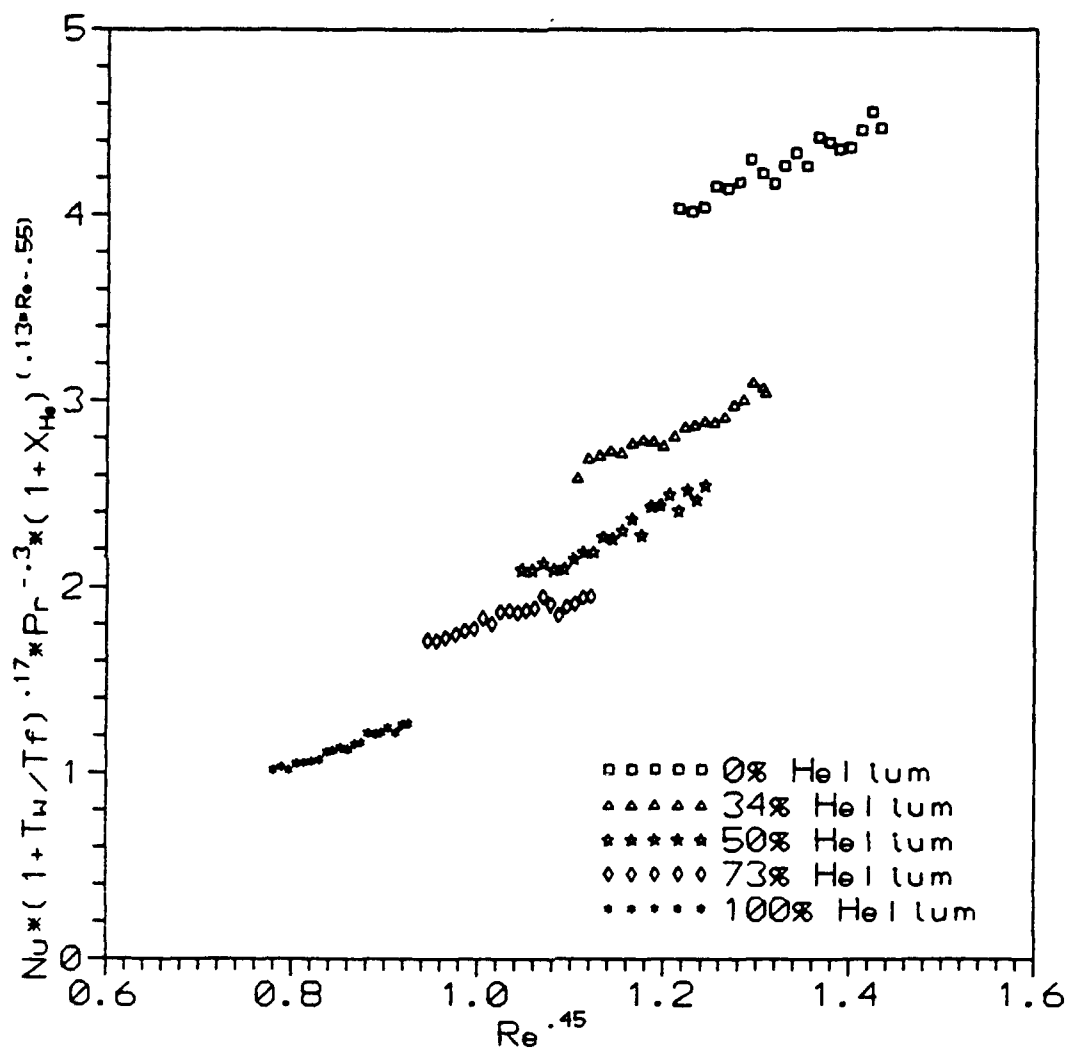


Figure 14. Tank Discharge Calibration Results  
Plotted using Equation 18

consistent effect of pressure on each concentration for the exponents used.

Figure 15 presents three different chamber pressures. The third order polynomial calibration curves shift to the right and up as the chamber pressure increases. This is to be expected since for a given concentration as the mass flow rate in the probe chamber increases, the Reynolds number increases. The y coordinate increases due to an increase in Reynolds number and Nusselt number. The Nusselt number increases due to an increase in heat transfer rate. The lines of constant concentration can be used to determine the helium molar concentration if the chamber pressure and Reynolds number or y coordinate are known. A major disadvantage of Figure 15 is that the calibration constants, A, B, C, and E of Equation 18 vary with chamber pressure.

By changing the exponent of term T2 in Equation 18 to the exponent of T2 in Equation 19, the curves collapse

$$\underbrace{Nu(1+\frac{T_w}{T_f})}_{T1}^{0.17} \underbrace{Pr^{-0.3}(1+X_{He})}_{T2}^{(0.8Re-0.55)} = \underbrace{A+BRe^{0.45}+CRe^{0.9}+ERe^{1.35}}_{T3} \quad (19)$$

to give a single curve as illustrated by Figure 16.

The third order polynomial curve fit equation is

$$y = 12.518 - 41.376 Re^{0.45} + 46.055 Re^{0.9} - 14.723 Re^{1.35}.$$

The calibration points are not as well behaved as desired.

The data scatter is believed to be due to instabilities in

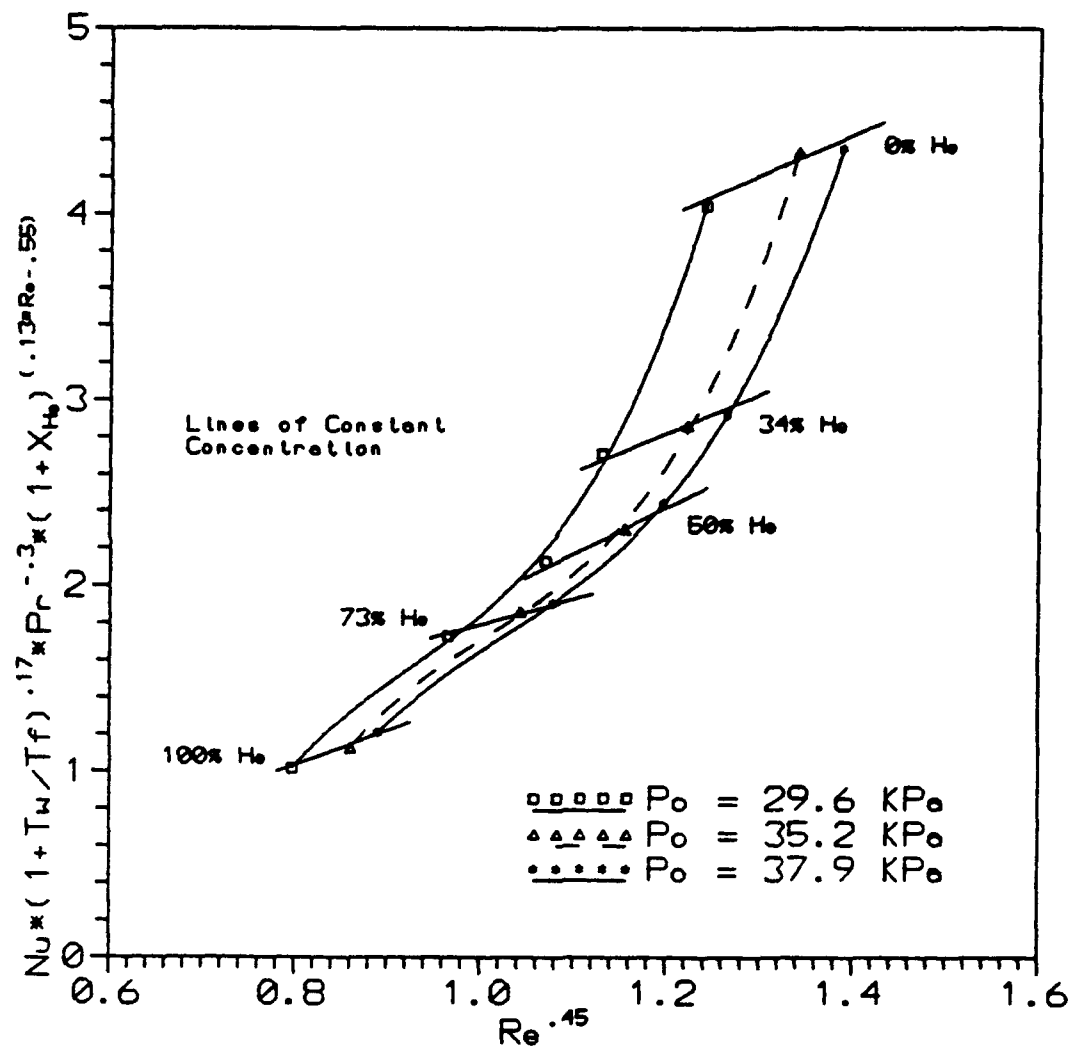


Figure 15. Pressure Effect, Tank Discharge Method



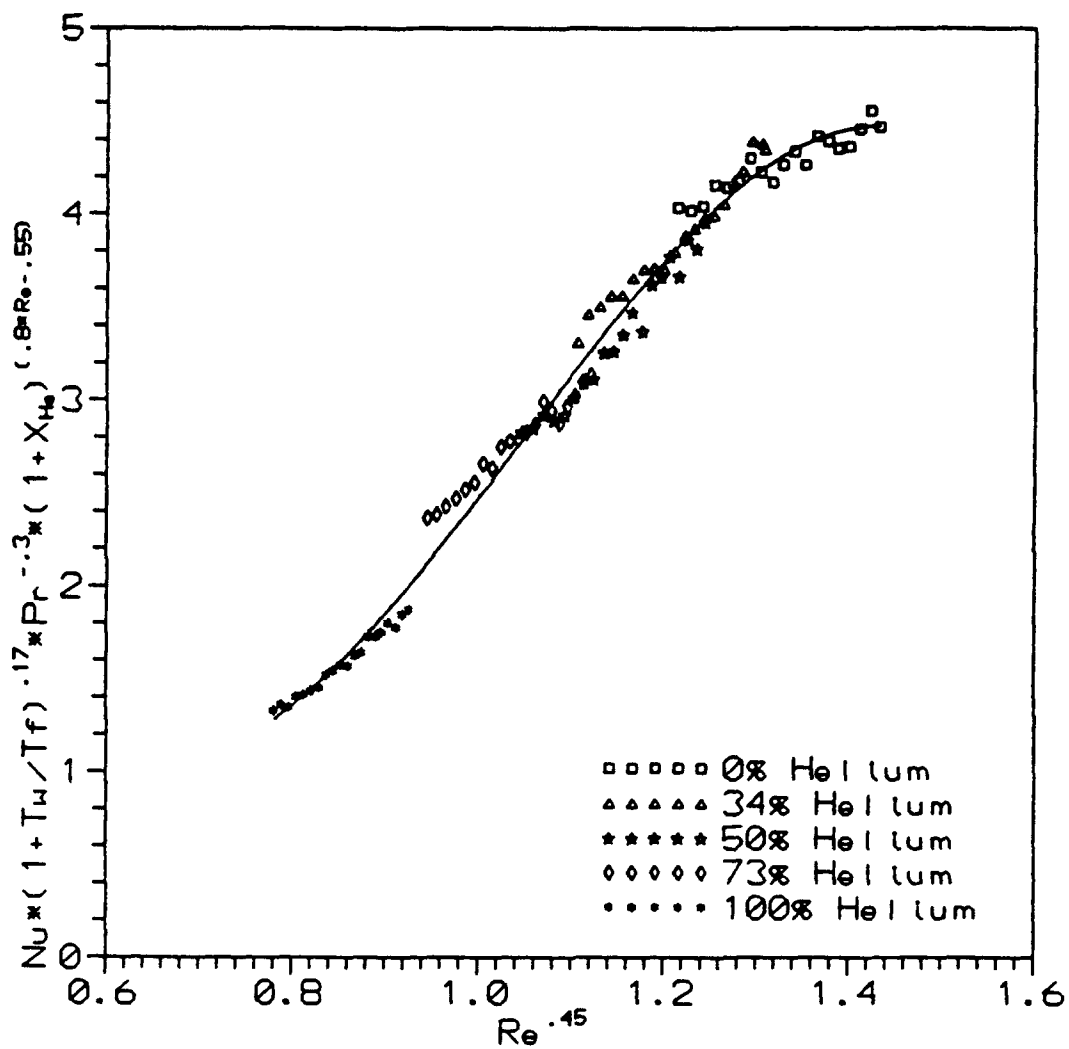


Figure 16. Tank Discharge Calibration Results  
Plotted using Equation 19

the hot wire bridge voltage. From Figure 16 the molar concentration can be calculated as follows:

- (1) Estimate the molar concentration of helium.
- (2) Calculate the mixture properties ( $C_p$ ,  $k$ ,  $R$ ,  $\gamma$ ,  $\mu$ ,  $\rho$ ) based on guessed helium concentration.
- (3) Calculate the mass flow rate using Equation 3.
- (4) Calculate the Nusselt, Reynolds, and Prandtl numbers using Equations 8, 13, and 14, respectively.
- (5) Determine if the right side and the left side of Equation 19 are equal.
- (6) If they match, stop; if they don't match, estimate the helium molar concentration again and repeat steps (1) - (5) (Tanis, 1993:63).

### 5.3 Steady Flow Calibration Results

The steady flow calibration method was conducted using two supersonic nozzles ( $\epsilon = 1.131$  and  $\epsilon = 2.778$ ). The results were first plotted with  $Re^{0.45}$  vs. the left side of Equation 18. Figure 17 shows the calibration results using the nozzle with an  $\epsilon$  value of 1.131 and a probe chamber pressure of 35.2 KPa. Figure 18 illustrates the calibration results using the supersonic nozzle with an  $\epsilon$  value of 2.778. The pressure effects are the same as with the tank discharge calibration results in that the calibration curves in Figure 18 move to the right and up with an increase in chamber pressure.

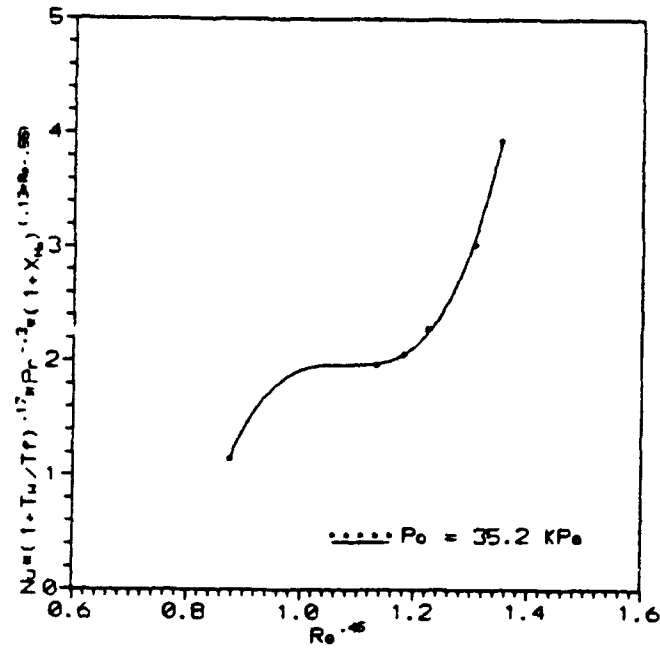


Figure 17. Steady Flow Calibration Results  
( $\epsilon = 1.131$ )

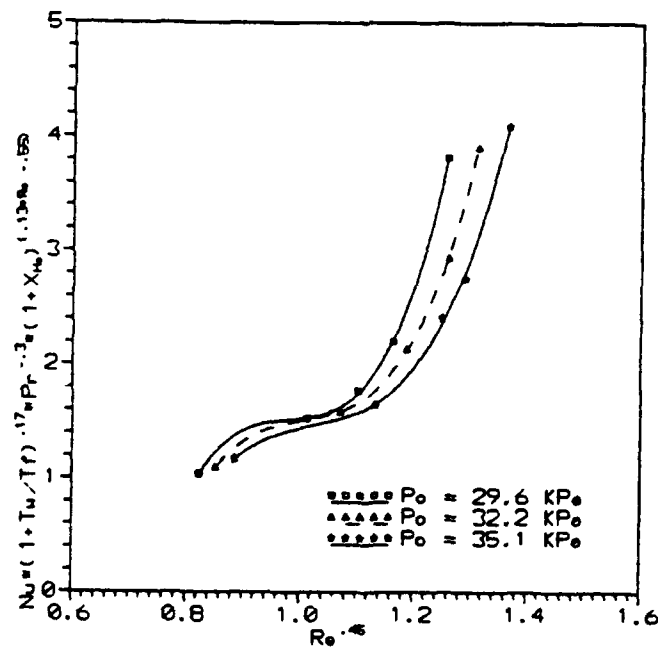


Figure 18. Steady Flow Calibration Results  
( $\epsilon = 2.778$ )

The major difference between the tank discharge results and steady flow results occurs in the center portions of the calibration curves. The third order polynomial calibration curves in Figures 17 and 18 have more curvature than those curves in Figure 15 of the tank discharge method. This trend may be attributed to variations in measured chamber temperature. Figures 19 and 20 show the chamber temperatures during calibration of the probe using the two supersonic nozzles ( $\epsilon = 1.131$  and  $\epsilon = 2.778$ , respectively). The figures indicate that the minimum fluid temperature decreases with an increase in Mach number.

Figure 21 is a comparison of the results from the tank discharge calibration method and steady flow calibration method where the chamber pressure is fixed at approximately 35.1 KPa. The difference between the tank discharge calibration results and steady flow calibration results may be attributed to a chamber temperature gradient. The temperature sensed in the chamber may be lower than the temperature of the fluid in the vicinity of the hot wire sensor. As the Mach number increases the difference between the actual and measured fluid temperature may be increasing. Recalling Equation 8

$$Nu = \frac{V_{br}^2 R_w d_w}{k_f A_{ref} (T_w - T_f) (R_w + R_b)^2} \quad (8)$$

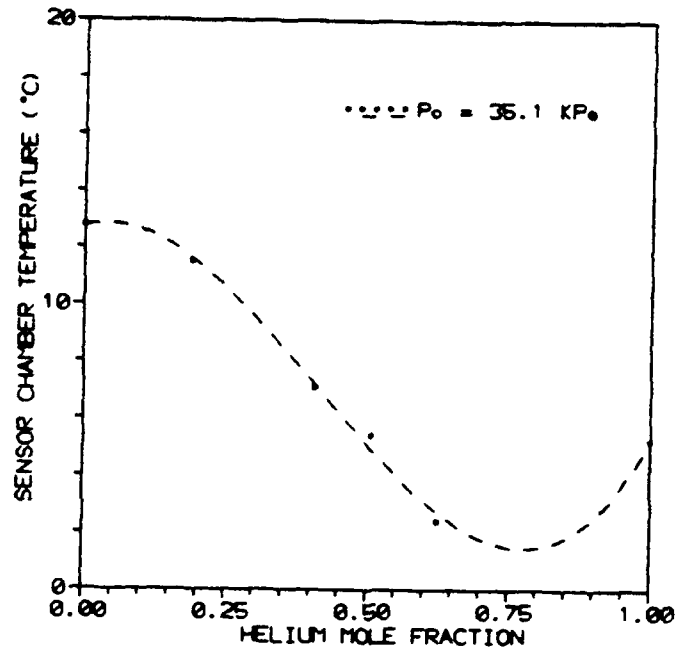


Figure 19. Temperature vs. Helium Concentration  
( $\epsilon = 1.131$ )

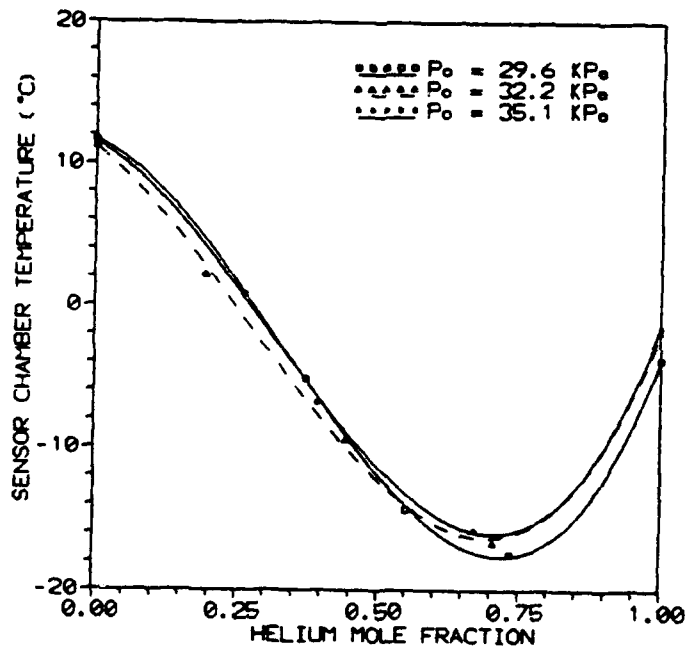


Figure 20. Temperature vs. Helium Concentration  
( $\epsilon = 2.778$ )

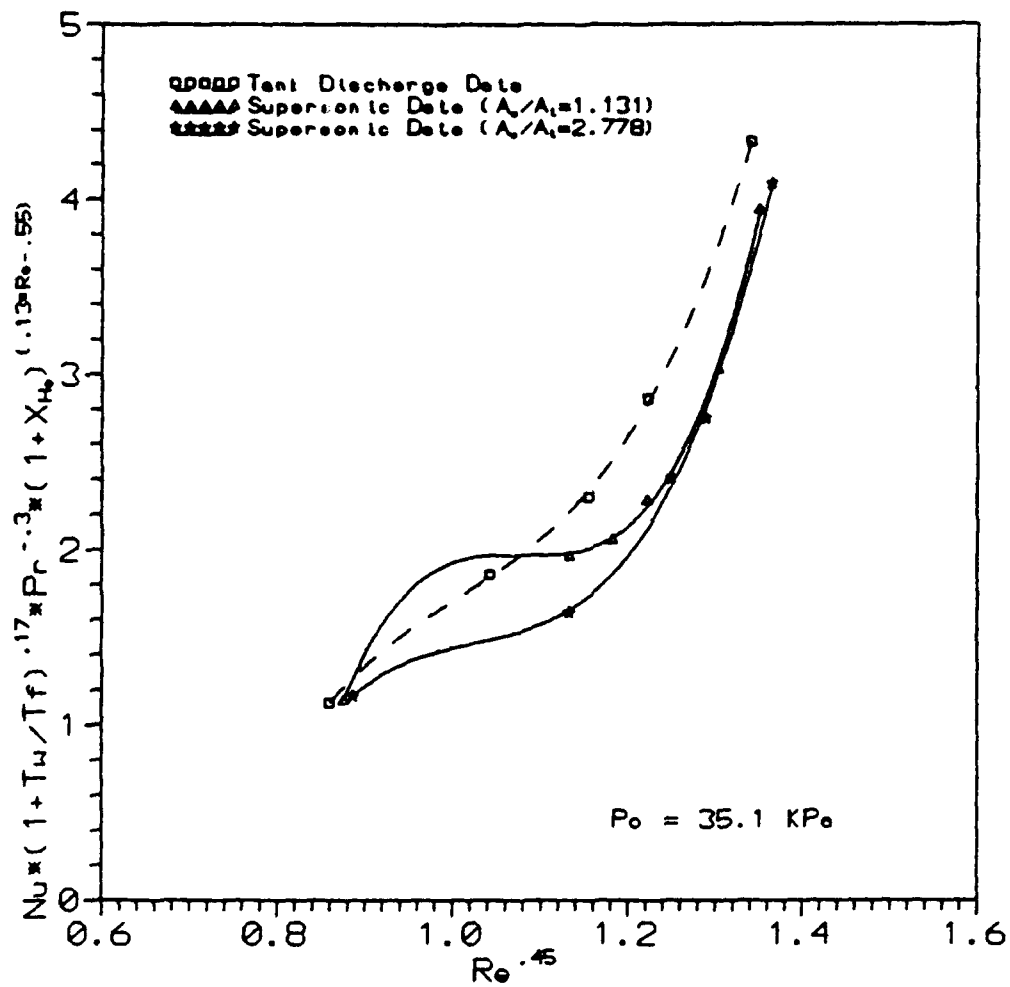


Figure 21. Comparison of Results of Tank Discharge Method and Steady Flow Method (Equation 18)

as  $T_r$  decreases, the Nusselt number (and  $y$  coordinate) decreases. The Nusselt number decreases faster than term  $T_1$  in Equation 18 increases. By making  $T_1$ 's exponent larger, the curves in Figure 21 would come together but the distance between overlapping points at 100 percent helium would increase.

Although not explored, an additional explanation for the difference between the tank discharge calibration results and steady flow calibration results focuses on the difference between the local total temperature and the adiabatic wall temperature. The difference between the two temperatures is a function of recovery factor, ratio of specific heats, and Mach number. Any further research should investigate the impact of the difference between the two temperatures on steady flow calibration results.

The steady flow calibration results might correlate better to the tank discharge calibration results if fluid temperature differences were eliminated. By heating the gas prior to entering the supersonic nozzle, the fluid temperature in the probe chamber could be controlled and kept constant. The heating of the gas should be investigated in any future steady flow calibration tests.

Equation 19 was also applied in generating calibration curves with the steady flow calibration method with good results. The calibration curves shown in Figures 22 and 23 for the two supersonic nozzles are quasi-linear and almost

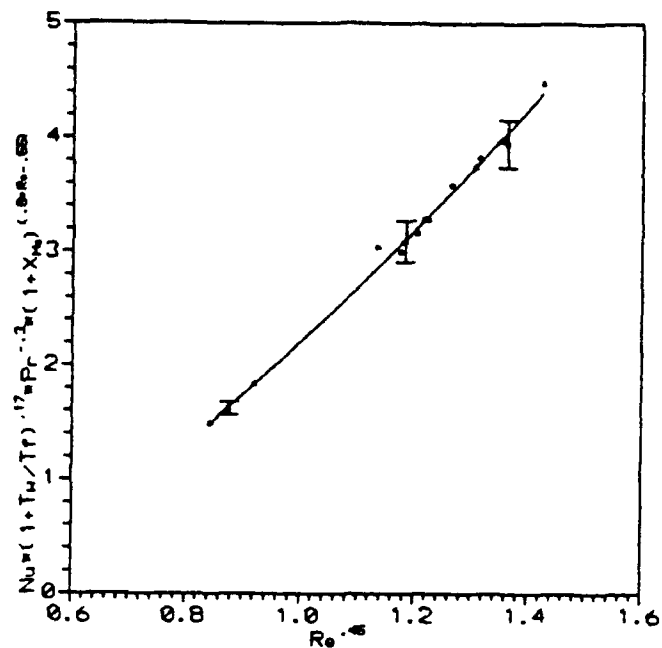


Figure 22. Steady Flow Results ( $\epsilon = 1.131$ ),  
Plotted using Equation 19.

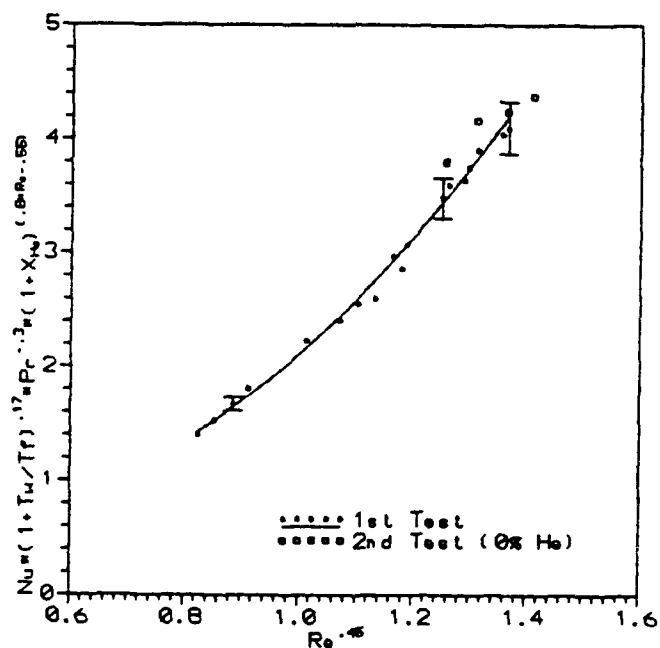


Figure 23. Steady Flow Results ( $\epsilon = 2.778$ ),  
Plotted using Equation 19



identical. The second order polynomial curve fit equation for Figure 22 is

$$y = -1.4892 + 2.6683 \text{ Re}^{0.45} + 1.0276 \text{ Re}^{0.9}$$

and for Figure 23 the curve fit equation is

$$y = 1.0571 - 2.3684 \text{ Re}^{0.45} + 3.4213 \text{ Re}^{0.9}.$$

The steady flow calibration method was repeated with the larger nozzle ( $\epsilon = 2.778$ ) with 100 percent air. The relative error between the first test and second test varied from 0.47 percent to 6.51 percent. The results of the second test are also shown in Figure 23. Two of the four values for the second test lie well within the error bars while the other two points call into question the repeatability of the probe.

A comparison between the results of the tank discharge method and steady flow method is exhibited in Figure 24. The steady flow results compare well to each other; however, the differences in shape of the tank discharge calibration curve versus the steady flow calibration curves is not understood. Future work should investigate possible causes for the difference.

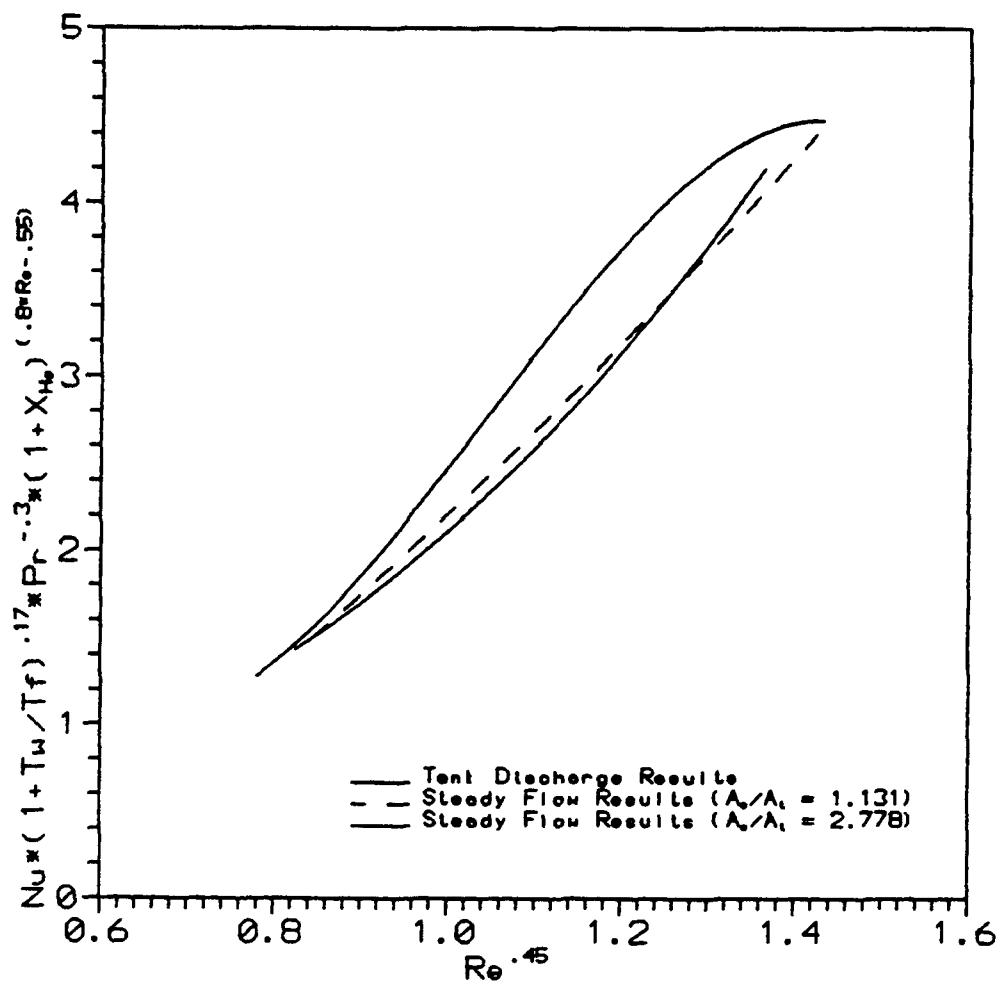


Figure 24. Comparison of Tank Discharge Results and Steady Flow Results (Equation 19)

## VI. Conclusions and Recommendations

### 6.1 Conclusions

The concentration probe shows promise in measuring binary gas concentrations in a supersonic flow field. It has excellent chamber pressure repeatability and stable temperature response required for accurate measurements. On the other hand, the probe is overly sensitive to changes in the probe cap temperature. This problem needs to be solved or at least understood and isolated. Additional tests need to be performed with other sensors and with additional nozzles to establish a firm foundation for comparison of the tank discharge calibration technique and the steady flow calibration technique.

### 6.2 Recommendations

The probe proved to be a useful instrument, but like most instruments, there is room for improvement.

Suggestions for improving the probe are:

- (1) Construct the probe body and probe cap out of a material much less conductive than brass.
- (2) Enlarge the cross sectional area of the probe chamber so that the thermocouple is further from the cap.
- (3) Build a pressure transducer into or close to the probe body to decrease the probe chamber response time.

Other recommendations include:

- (1) Study the dynamics of the inner geometry of the probe cap (i.e. how it affects shock wave position and, thus, probe chamber pressure).
- (2) Study the regions around the chamber thermocouple and pressure port entrance to determine if they are regions of recirculation and if so how they affect total temperature and total pressure.
- (3) Add a heater in the vicinity of the stilling chamber to control the fluid temperature of the gas flowing past the probe.
- (4) Further study the effects of back pressure on probe chamber temperature.

## References

- Adler, D. "A Hot-Wire Technique for Continuous Measurement in Unsteady Concentration Fields of Binary Gaseous Mixtures," Journal of Physics E, 5: 163-169 (1971)
- ASME Fluid Meters: Their Theory and Applications. Edited by Howard S. Bean. New York: ASME, 1971.
- Bird, R., Stewart, W.E. and Lightfoot, E. N. Transport Phenomena. New York: John Wiley and Sons, Inc., 1960.
- Blackshear, Perry L. and Leroy Fingerson. "Rapid Response Heat Flux Probe for High Temperature Gases," American Rocket Society Journal, 32: 1709-1715 (November 1962)
- Brown, G. L. and M. R. Rebello. "A Small Fast Response Probe to Measure Composition of a Binary Gas Mixture," AIAA Journal, 10: 649-652 (May 1972)
- Collis, D. C. and Williams, M. J. "Two-Dimensional Convection from Heated Wires at Low Reynolds Number," Journal of Fluid Mechanics, 6: 357-384 (October 1959)
- IFA-100 Users Manual, Thermal Systems Incorporated, 1985.
- Ng, W. F., F. T. Kwok, and T. A. Ninnemann. "A Concentration Probe for the Study of Mixing in Supersonic Shear Flows," AIAA/ASME/SAE/ASEE 25th Joint Propulsion Conference: AIAA-89-2459 (July 1989)
- Shapiro, A. H. The Dynamics and Thermodynamics of Compressible Fluid Flow. New York: John Wiley and Sons, 1953.
- Stoller, Capt George R. Development of an Alternative Concentration Probe Calibration Method. MS Thesis AFIT/GAE/ENY/89D-37. School of Engineering, Air Force Institute of Technology (AU), Wright-Patterson AFB OH, December 1989.
- Tanis, F. An Experimental Study of Planar Heterogeneous Supersonic Confined Jets. Unpublished PhD dissertation. Air Force Institute of Technology, OH, 1993.
- Taylor, J. R. An Introduction to Error Analysis. Mill Valley CA: University Science Books, 1982.
- Zakanycz, S. Turbulence and the Mixing of Binary Gases. PhD dissertation. Ohio State University, OH, 1971.

## Appendix A. Venturi Calibration

The venturi required calibration to determine its discharge coefficient. The discharge coefficient of the square-edge orifice plate was determined using the following series of equations (ASME, 1971:52-201)

$$C_d = K\sqrt{1-\beta^4} \quad (20)$$

where  $\beta$  = ratio of diameters,  $d/D$ . The variable,  $K$ , is defined by Equation 21

$$K = K_o(1 + \frac{F}{R_d}) \quad (21)$$

and  $K$  is further broken down into Equations 22 - 24.

$$K_o = K_o(\frac{10^6 d}{10^6 d + 15F}) \quad (22)$$

$$\begin{aligned} K_o = & 0.5993 + \frac{0.007}{D} + (0.364 + \frac{0.076}{\sqrt{D}}) \beta^4 \\ & + 0.4(1.6 - \frac{1}{D})^5 [(0.07 + \frac{0.5}{D}) - \beta]^{2.5} \\ & - (0.009 + \frac{0.034}{D}) (0.5 - \beta)^{1.5} \\ & + (\frac{65}{D^2} + 3) (\beta - 0.7)^{1.5} \end{aligned} \quad (23)$$

$R_d$  is the Reynolds number at the square-edged orifice and  $F$  is defined by

$$F = d(830 - 5000\beta + 9000\beta^2 - 4200\beta^3 + \frac{530}{\sqrt{D}}) \quad (24)$$

Note: If any of the last three terms in Equation 23 reduces to an imaginary number that term or terms are dropped.

The actual mass flow rate through the square-edged orifice is determined by

$$\dot{m}_{\text{orifice}} = \frac{\pi Y_1 d^2}{4} \frac{C_d}{\sqrt{1-\beta^4}} \sqrt{2g_c \rho_1 (p_1 - p_2)} \quad (25)$$

and

$$Y_1 = 1 - (0.410 + 0.350\beta^4) \frac{z}{Y} \quad (26)$$

where  $z = 1 - p_2/p_1$ . The theoretical mass flow rate through the venturi is determined by

$$\dot{m}_{\text{chvent}} = aY \sqrt{\frac{2g_c \rho_1 (p_1 - p_2)}{1-\beta^4}} \quad (27)$$

where  $Y$  is

$$Y = [r^{2/\gamma} \left( \frac{Y}{Y-1} \right) \left( \frac{1-r^{\frac{\gamma-1}{\gamma}}}{1-r} \right) \left( \frac{1-\beta^4}{1-\beta^4 r^{2/\gamma}} \right)]^{1/2} \quad (28)$$

The value  $a$  is the cross sectional area of the venturi throat and  $r = p_2/p_1$ . The discharge coefficient of the venturi tube is finally calculated by Equation 29.

$$C_{d \text{ vent}} = \frac{m_{\text{orifice}}}{m_{\text{thvent}}} \quad (29)$$

The discharge coefficient of the venturi was calculated to be 0.984.



## Appendix B. Thermal Resistance Coefficient

Sensor resistance versus sensor temperature is plotted to determine the thermal resistance coefficient. The thermal resistance coefficient is required to calculate the operating temperature of the hot wire sensor. The correlation factor of the plotted data is 0.9997.

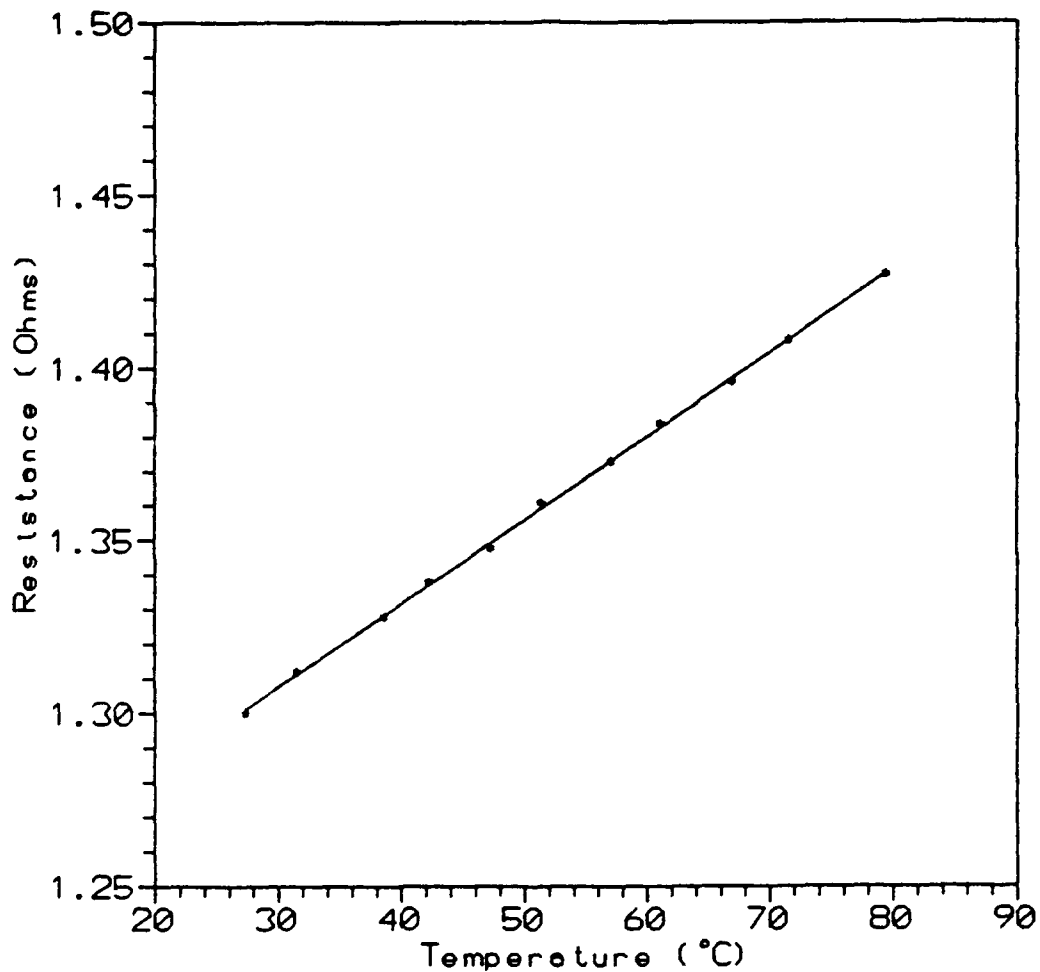


Figure 25. Sensor Resistance vs. Temperature

### Vita

Captain John S. Alsup was born on 13 December 1960 in Cheyenne, Wyoming. He graduated from Austin High School in Decatur, Alabama in 1979. He began his engineering studies at John C. Calhoun Community College in Decatur, then transferred to Brigham Young University in Provo, Utah. In 1984 he joined the enlisted ranks of the Air Force. While working as an Aircraft Machinist at George AFB, California, he was accepted into the Airman's Education and Commissioning Program. He attended Oklahoma State University where he graduated in May 1989 with a Bachelor of Science in Mechanical Engineering degree. Upon graduation, he went to Officer Training School and was commissioned as a Second Lieutenant in the United States Air Force. After serving as a Technical Engineer at F.E. Warren AFB, Wyoming, for two and one half years, Capt Alsup reported for training to the Air Force Institute of Technology in May 1992.

Permanent Address: 643 N. 700 E.  
Firth, Idaho 83236

# REPORT DOCUMENTATION PAGE

Form Approved

OMB No. 0704-0188

Public reporting burden for this collection of information is estimated to average 1 hour per response, including the time for reviewing instructions, searching existing data sources, gathering and maintaining the data needed, and completing and reviewing the collection of information. Send comments regarding this burden estimate or any other aspect of this collection of information, including suggestions for reducing this burden, to Washington Headquarters Services, Directorate for Information Operations and Reports, 1215 Jefferson Davis Highway, Suite 1204, Arlington, VA 22202-4302, and to the Office of Management and Budget, Paperwork Reduction Project (0704-0188), Washington, DC 20503.

1. AGENCY USE ONLY (Leave blank)

2. REPORT DATE

December 1993

3. REPORT TYPE AND DATES COVERED

Master's Thesis

4. TITLE AND SUBTITLE

EVALUATION OF A CONCENTRATION PROBE FOR APPLICATION IN A SUPERSONIC FLOW FIELD

5. FUNDING NUMBERS

6. AUTHOR(S)

John S. Alsup, Captain, USAF

7. PERFORMING ORGANIZATION NAME(S) AND ADDRESS(ES)

Air Force Institute of Technology, WPAFB OH 45433-7765

8. PERFORMING ORGANIZATION REPORT NUMBER

AFIT/GAE/ENY/93D-3

9. SPONSORING MONITORING AGENCY NAME(S) AND ADDRESS(ES)

Dr. Richard B. Rivir  
WL/POTC  
1950 5th Street, Bldg 18  
WPAFB OH 45433-7251

10. SPONSORING / MONITORING AGENCY REPORT NUMBER

11. SUPPLEMENTARY NOTES

12a. DISTRIBUTION / AVAILABILITY STATEMENT

Approved for public release; distribution unlimited

12b. DISTRIBUTION CODE

13. ABSTRACT (Maximum 200 words)

Aspirating, concentration probes are used to measure binary gas concentrations in a supersonic flow. In the past, a tank discharge method has been used to calibrate concentration probes. An alternate calibration method has been developed and tested on a probe in a steady, subsonic/sonic flow. This study evaluated the calibration and performance of a concentration probe in a steady, supersonic flow over a range of mixture ratios of air and helium. The results of this study and a comparison of the two calibration methods are presented.

14. SUBJECT TERMS

Anemometers, Hot Wire Anemometers,  
Calibration, Probes, Supersonic Flow

15. NUMBER OF PAGES

67

16. PRICE CODE

17. SECURITY CLASSIFICATION OF REPORT

Unclassified

18. SECURITY CLASSIFICATION OF THIS PAGE

Unclassified

19. SECURITY CLASSIFICATION OF ABSTRACT

Unclassified

20. LIMITATION OF ABSTRACT

U